

Dynamics of quantum phase transitions in Dicke and Lipkin-Meshkov-Glick models

A.P. Itin^{1,2} and P. Törmä¹

¹*Department of Applied Physics, Aalto University, P.O. Box 15100, 00076, Finland*

²*Space Research Institute, RAS, Profsoyuznaya str. 84/32, 117997 Moscow, Russia*

We consider dynamics of Dicke models, with and without counterrotating terms, under slow variations of parameters which drive the system through a quantum phase transition. The model without counterrotating terms and swept detuning is seen in the contexts of a many-body generalization of the Landau-Zener model and the dynamical passage through a second-order quantum phase transition (QPT). Adiabaticity is destroyed when the parameter crosses a critical value. Applying semiclassical analysis based on concepts of classical adiabatic invariants and mapping to the second Painleve equation (PII), we derive a formula which accurately describes particle distributions in the Hilbert space at wide range of parameters and initial conditions of the system. We find striking universal features in the particle distributions which can be probed in an experiment on Feshbach resonance passage or a cavity QED experiment. The dynamics is found to be crucially dependent on the direction of the sweep. The model with counterrotating terms has been realized recently in an experiment with ultracold atomic gases in a cavity. Its semiclassical dynamics is described by a Hamiltonian system with two degrees of freedom. Passage through a QPT corresponds to passage through a bifurcation, and can also be described by PII (after averaging over fast variables), leading to similar universal distributions. Under certain conditions, the Dicke model is reduced to the Lipkin-Meshkov-Glick model.

I. INTRODUCTION

Adiabatic invariance is a central issue in both quantum and classical mechanics. Magnitudes that we call now "adiabatic invariants" appeared for the first time in works of L.Boltzmann (see, e.g., [1]). The term "adiabatic invariant" itself was introduced by P. Ehrenfest [2, 3]. Study of changes in the adiabatic invariants and their relation to quantum nonadiabatic transitions was started, presumably, by P.A.M. Dirac [4]; early attempts to formulate and prove quantum adiabatic theorem were done on the eve of quantum mechanics [5, 6]. Since then, destruction of adiabaticity in quantum and classical contexts has been subject of research for decades, with recent explosive revival of interest to that theme due to experiments with ultracold quantum gases [7, 8].

For a single-particle quantum system, very often nonadiabatic dynamics can be described within the exactly solvable Landau-Zener model (LZM) [9], where a probability of transition from an initially occupied instantaneous ground state level to the excited one is exponentially small in the parameter describing the sweeping rate of the detuning between the levels.

Ultracold quantum gases experiments may involve macroscopically large numbers of particles, making semiclassical (*SC*) treatments justified (see, e.g., [10–13]). Nonadiabatic dynamics in *SC* models of many-particle systems has been intensively discussed recently (see [12, 14] and references therein). In many treatments, it was found that exponential LZM-type behaviour for the transition probabilities is replaced with power-laws of the sweeping rates.

A universal and accurate method for describing nonadiabatic *SC* dynamics of such many-particle quantum systems was presented by us recently [14]. The method is based on (i) replacing a quantum state with ensemble

of classical trajectories distributed according to a Wigner function [15] of the initial state (ii) propagating this ensemble and (iii) mapping its dynamics near a bifurcation to a Painleve equation. For (i),(ii), we follow Altland et al [12] (in the present paper we also introduce certain modifications coming from SU(2) Wigner function formalism for spin systems [16, 17]). Stage (iii) is not trivial. If initial state is chosen to be far from the ground state, then initial classical actions are not very small, and general separatrix crossing theory can be applied to calculate the deviation from adiabaticity. For small initial actions, mapping to a Painleve equation is necessary.

Thus, an interesting relation between many-particle Landau-Zener models, Wigner functions, dynamics of quantum phase transitions and *Painleve equations* [18] was established. The Painleve equations have found many applications in quantum field theory and other areas of physics (for example, they describe correlation functions of certain fermion models [19]). They possess a property that makes them in some respect similar to linear differential equations: the Painleve property (also called Fuchs-Kovalevskaya-Painleve property in Russian literature). That is, their solutions have only simple poles as movable (dependent on initial conditions) singularities in the complex time plane. Since works of Kovalevskaya [20] this property is known to be useful to find integrable systems. Using the method of isomonodromic deformations, it is possible to construct asymptotics of the Painleve equations and *connection formulae* (which we utilize in the present paper, following [21]) by a modification of the WKB method for linear differential equations [19].

In this article, we elaborate the method [14] further, implementing it for the Dicke model [22] with counterrotating terms and dissipation, and Lipkin-Meshkov-Glick (LMG) model [23], and show that peculiar properties of

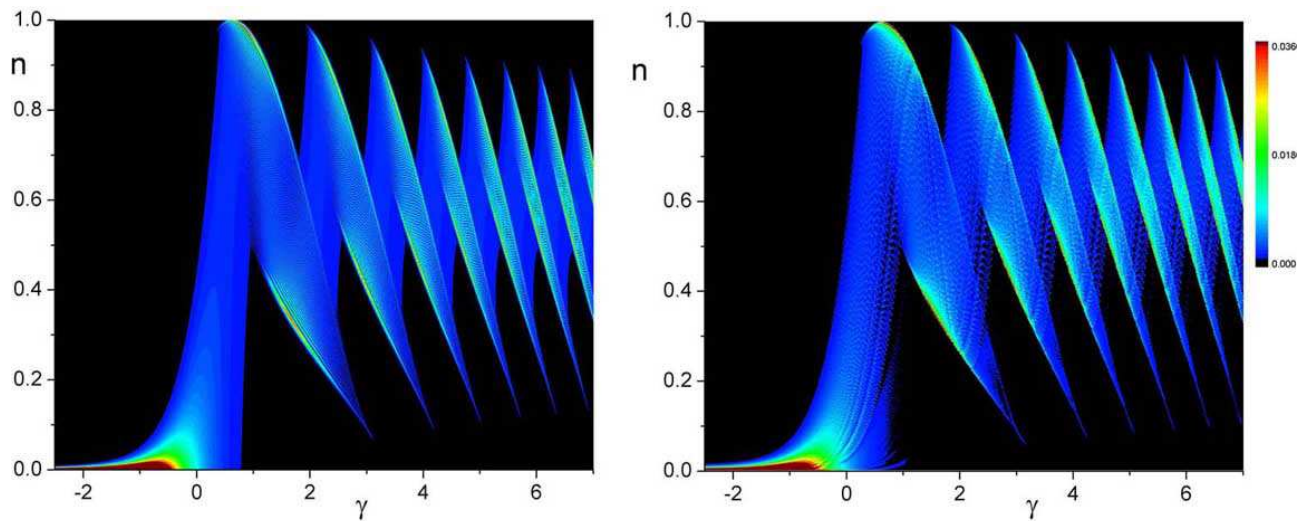


FIG. 1: The time evolution of the distribution of the rescaled boson number n at a "forward" sweep through the resonance. (a) Numerical quantum calculation with $N=500$ (according to Eqs.1,2). (b) Corresponding ensemble of classical trajectories; the sweeping rate is $\epsilon = 0.3$.

PII can appear in experiments with cold atoms. LMG model arises, in particular, as an effective model at certain range of parameters in an experiment recently done by the group of T.Esslinger [24, 25]. Other experimental realizations of LMG model were also suggested [26]. On the basis of Dicke model with counterrotating terms we confirm that the method works for systems whose classical counterpart is a few-dimensional Hamiltonian system experiencing a pitchfork bifurcation at a critical value of a parameter.

In the next section, we describe the Dicke model without counter-rotating terms and its connection to applications.

Section III considers a passage through the quantum phase transition in the LMG model. We note, following Keeling et al. [24], that in the Dicke model *with counterrotating terms* under conditions relevant to the experiment [25], LMG model arises as an effective model after adiabatic elimination of the photon field. Dynamics of quantum phase transitions is studied, and the universal distributions after the sweep of the parameter are found.

Section IV considers Dicke model with counterrotating terms [22] and comparable frequencies of the photon field mode and the two-state system (i.e., separation of timescales of Section III allowing mapping to LMG model does not happen here). In this model, a quantum phase transition between normal and superradiant phases was studied [27]. Also, signatures of quantum chaos were investigated [27]. We analyze the *dynamics* of the quantum phase transition. The corresponding classical Hamiltonian system has two degrees of freedom; this, in particular, leads to chaotization of large area of phase space in the "superradiant" phase. Naively, it should preclude the application of our method. However we demonstrate that the passage through a bifurcation happens in a one-

dimensional way and can be also described by PII. For not very fast sweeps, most of the classical wavepacket will remain in the vicinity of new equilibria. There, the phase space is regular: one may introduce classical actions and modify the method of Sections II-III correspondingly.

Section V presents the conclusions.

II. NON-ADIABATICITY OF A MANY-PARTICLE LANDAU-ZENER PROBLEM: FORWARD AND BACKWARD SWEEPS

A. The time-dependent Dicke model without counterrotating terms as a many-particle LZM

We consider the following many-particle LZM: time-dependent Dicke model [22] which has numerous applications in quantum and matter-wave optics [12, 13, 31]. The model can be written as

$$\hat{H} = -\frac{\gamma(t)}{2}\hat{b}^\dagger\hat{b} + \frac{\gamma(t)}{2}\hat{S}^z + \frac{g}{\sqrt{N}}(\hat{b}^\dagger\hat{S}^- + \hat{b}\hat{S}^+), \quad (1)$$

where $\frac{g}{\sqrt{N}}$ is the coupling strength, $\hat{S}^\pm = \hat{S}_x \pm i\hat{S}_y$ are spin operators, \hat{b}^\dagger and \hat{b} are creation and destruction operators of a bosonic mode, $\gamma(t) = \pm 2\epsilon t$ is the detuning from the resonance, and ϵ is the sweeping rate of the bosonic mode energy. The spin value S can be considered macroscopically large $S = N/2 \gg 1$; usually the physical origin of the effective spin variable S is a collection of two-level systems (spin-1/2 particles). Among many possible applications, let us mention the Feshbach resonance passage [8, 28–32], dynamics of molecular nanomagnets [33], and cavity QED with Bose-Einstein condensates (BEC) [12, 24].

With $N = 1$, one recovers the standard Landau-Zener model. In the context of a Feshbach resonance passage in a Fermi gas, an equivalent realization of the Hamiltonian (1) is

$$\hat{H} = \frac{\gamma(t)}{2} \sum_{i=1}^N (\hat{n}_{i\uparrow} + \hat{n}_{i\downarrow}) + \frac{g}{\sqrt{N}} \sum_{i=1}^N (\hat{b}^\dagger \hat{c}_{i\downarrow} \hat{c}_{i\uparrow} + h.c.),$$

where $\hat{c}_{i,\sigma}$ and \hat{b} are the fermion and boson annihilation operators, respectively, $\hat{n}_{i\sigma} = \hat{c}_{i\sigma}^\dagger \hat{c}_{i\sigma}$, and $\sigma = \uparrow, \downarrow$. Coupled atom-molecular BECs are described by a similar model whose dynamics in the limit of large N becomes equivalent to (1) with the replacement $\gamma \rightarrow -\gamma$ [12, 14]. That is, in the thermodynamic limit of the degenerate model (1) association of fermionic atoms becomes near equivalent to dissociation of a molecular BEC, and vice versa. We discuss two driving scenarios here: "forward" and "backward" sweeps.

In the "forward" sweep, starting in the distant past with some small initial number of bosons $N_b(t)|_{-\infty} \equiv \langle \hat{b}^\dagger \hat{b} \rangle(t)|_{-\infty} = N_- \equiv \mathbf{n}_- N$, we want to calculate the final number of bosons $N_b(t)|_{+\infty} \equiv \bar{n} N$ and its distribution $P(\bar{n})$ as a function of the sweeping rate ϵ and the initial bosonic fraction \mathbf{n}_- . To be more specific, in the infinite past we start in a (Dicke) eigenstate of (1): $|\psi_{-\infty}\rangle = |N_-\rangle |S, S_z\rangle = |N_-\rangle |\frac{N}{2}, \frac{N}{2} - N_-\rangle$, where N_- can be zero in case we start at the ground state. We consider the sector $S = N/2$ for clarity, but other values of S can be treated analogously (Hilbert space of (1) is decoupled on sectors with definite total spin, or "cooperation number", S). Matrix elements of (1) have the form

$$H_{n,n'} = -\gamma(t) \delta_{n,n'} + n \delta_{n,n'+1} \sqrt{N-n'}/\sqrt{N} \quad (2) \\ + n' \delta_{n,n'-1} \sqrt{N-n}/\sqrt{N}$$

(we use $g = 1$ for convenience in this paper, which can always be achieved by rescaling of time), therefore the model can be referred to the class of generalized Landau-Zener models [34] in the case of linear driving $\gamma(t) \sim t$.

In the second dynamical scenario ("backward"), we start in the ground state of (1) at large positive value of γ and make an "inverse" sweep to large negative γ (see also [14]). This scenario is relevant to association of Bose atoms to a molecular BEC [12]. On a purely classical level, there is a drastic asymmetry in the forward and backward sweeps. Starting in the classical ground state of (9) at $\gamma = -\infty$ (i.e. $n = 0$, "all-atom" mode in context of Fermi association), one obtains a situation where dynamics is absent: a phase point always remains in the equilibrium. To trigger dynamics, one needs either to consider nonzero initial population of the molecular mode (as done, in particular, in [13]), or carefully take into account quantum fluctuations [12]. This should be contrasted with the "backward" sweep [14], where, starting in the classical ground state at $\gamma = +\infty$ (i.e., $n = 1$, "all-atom" mode in context of Bose atoms association and "all-molecule" mode in context of Fermi association),

there will be dynamics, and the system can be considered on a purely classical level [12, 14]. Such asymmetry in classical dynamics with respect to direction of sweeps is preserved on a semiclassical level as well, as will be shown below.

The Dicke model [22] and its equivalent realizations have been studied already using various techniques. Diagrammatic methods employed in [12] work well for small N but do not allow to get close to the SC limit for large N . Another approach is a SC treatment based on classical adiabatic invariants (see [12, 13] and references therein). At $|t| = \infty$ and $N \rightarrow \infty$ the relative number of bosons N_b/N corresponds to a classical action I of an effective Hamiltonian system, so that for large but finite N the problem can be mapped to the calculation of a change of classical actions of a properly prepared ensemble of trajectories. It is inspiring that calculations with ensembles of classical trajectories (defined below) reproduce full quantum calculations very well (see Fig.1).

B. Classical ensembles and quantum dynamics

1. Classical limit of the system

The classical limit of (1) can be obtained from the Heisenberg equations of motion by factoring all operator products:

$$\begin{aligned} \dot{x} &= -\frac{\gamma}{2} y - g z p, \\ \dot{y} &= \frac{\gamma}{2} x - g z e, \\ \dot{z} &= g(x p + y e), \\ \dot{e} &= -\frac{\gamma}{2} p - g y, \\ \dot{p} &= \frac{\gamma}{2} e - g x, \end{aligned} \quad (3)$$

where the variables x, y, z are components of the Bloch vector, while p, e are the components of the boson ("radiation") field:

$$p = \frac{i}{\sqrt{N}} (b^* - b), \quad e = \frac{1}{\sqrt{N}} (b + b^*), \\ x, y, z = \frac{2}{N} S_{x,y,z}. \quad (5)$$

The length of the Bloch vector $x^2 + y^2 + z^2 = 1$ is the integral of motion. The equations (3) are equivalent to the Hamiltonian equations of motion of the following Hamiltonian:

$$H = \frac{\gamma}{2} (z - I) - g \sqrt{2I} \sqrt{1 - z^2} \sin(\theta - \phi), \quad (6)$$

where (z, θ) and (I, ϕ) are canonically conjugated pairs of variables related to the variables of (3) by

$$x = \sqrt{1 - z^2} \cos \theta,$$

$$\begin{aligned}
y &= \sqrt{1-z^2} \sin \theta, \\
p &= \sqrt{2I} \cos \phi, \\
e &= \sqrt{2I} \sin \phi.
\end{aligned} \tag{7}$$

Eqs.(3) possess an additional integral of motion: $\tilde{L} = I + z$, which makes the Hamiltonian (6) at constant γ integrable. Switching from the variables (I, ϕ) , (z, θ) to $(\tilde{L} = I + z, \tilde{\theta} = \theta)$, $(\tilde{n} = I, \tilde{\phi} = \phi - \theta)$, one obtains $H = -\gamma\tilde{n} + g\sqrt{2\tilde{n}}\sqrt{1 - (\tilde{L} - \tilde{n})^2} \sin \tilde{\phi}$. Denoting $\tilde{n} = 2n$, $1 - \tilde{L} = 2L$, shifting the phase $\tilde{\phi} = \phi - \pi/2$, rescaling H by a factor of 2 and setting $g = 1$ one obtains

$$H = -\gamma n - 2\sqrt{n(n+L)(1-L-n)} \cos \phi, \tag{8}$$

where $n \in [0, 1]$ corresponds to the rescaled number of bosons N_b/N , and ϕ is the canonically conjugated phase.

2. Classical distribution

Distributions of n, ϕ as well as distribution of integral of motion L follow from the initial Wigner function of the system. There are at least two different ways to define Wigner function of the system: using decomposition of spin on Schwinger bosons leads to highly oscillatory Wigner function from which an effective positive distribution should be derived [12, 14], while implementing SU(2) Wigner function for spin system [16, 17] immediately gives positive Wigner distribution of the initial state because both eigenstates of \hat{S}_z with maximal absolute values of S_z , $|\pm S, S\rangle$ possess positive, non-oscillatory Wigner function. Interesting enough, we found that in the limit of large N both approaches give the same results: SU(2) Wigner function leads to the same exponential distributions as that used in [12, 14]. Indeed, as shown in [17] the eigenstate $|\frac{N}{2}, \frac{N}{2}\rangle$ has SU(2) Wigner function $W_{\frac{N}{2}}(\Theta) \approx \cos^N \Theta [1 + \cos \Theta] = z^N (1+z)$ (see Appendix), where Θ is an angle on Bloch sphere: $z = \cos \Theta$. This function at large N is asymptotically close to exponential: $z^N (1+z) \approx 2 \exp[-(1-z)N]$.

On the other hand, the approach used in [14] is as follows. The classical limit of (1) can be also obtained by introducing Schwinger bosons $\hat{\alpha}, \hat{\beta}$: $\hat{S}^+ = \hat{\alpha}^\dagger \hat{\beta}$, $\hat{S}^- = \hat{\beta}^\dagger \hat{\alpha}$, $\hat{S}_z = (\hat{n}_\alpha - \hat{n}_\beta)/2$, and using the c -number formalism [12, 13]. The resulting classical system has 3 pairs of variables $(n_{\alpha,\beta,b})$ and conjugated phases $(\theta_{\alpha,\beta,b})$ and 2 integrals of motion ($N_\alpha \equiv n_\alpha + n_\beta$, $L \equiv n_\beta - n_b$). To obtain the Wigner function, one notes that far from the resonance, the quantum system is effectively decoupled on 3 oscillators, 2 of them being in the ground state, and the third one in the high-lying Fock state $|N\rangle$. With a good accuracy, $W(n_{b,\alpha,\beta}) \sim \exp(-2n_b - 2n_\beta) \delta(n_\alpha - 1)$. The origin of such distribution is as follows. Wigner function of the ground state of an oscillator is $W_0 = 2 \exp(-2n_{b,\beta})$. Wigner function of a highly lying Fock state is highly oscillatory and, in principle, is not suitable

for preparation of a classical distribution we need. However, the effective smooth distribution (Gaussian) was derived by Gardiner et al. [35], and it is much narrower than the distribution of the ground state. Therefore, with a good accuracy it can be replaced with the delta-function, as authors of [12, 36] did. In all distributions mentioned above, phases $\theta_{\alpha,\beta,b}$ are uniformly distributed on $[0, 2\pi]$. It means initial phase ϕ is also uniformly distributed on $(0, 2\pi)$; also, besides exponential distribution of initial n , we have to take into account distribution of the parameter L .

3. Nonadiabatic dynamics of classical trajectories

Let us now analyze the classical trajectories from the initial distribution. Consider firstly the case $L = 0$, then the Hamiltonian reduces to

$$H = -\gamma n - 2n\sqrt{1-n} \cos \phi. \tag{9}$$

Note that by means of a trivial change of variables [37], the Hamiltonian becomes the same as analyzed e.g. in [13]. The classical phase space of the Hamiltonian (9) at fixed values of the parameter γ is described in [13, 14]. If $\gamma < -2$, there is only one stable elliptic point on the phase portrait (Fig.2a). At $\gamma = -2$, a bifurcation takes place. There are two saddle points at $n = 0, \cos \phi = -\gamma/2$, and a newborn elliptic point at $\phi = 0$. The trajectory connecting these two saddles (the separatrix) separates rotations and oscillating motions. At large positive γ , again there is only one elliptic stationary point at $\phi = 0$, and n close to 1. The classical action is defined as in [12, 13] and is shown graphically in Fig. 3: shaded areas, divided by 2π . At $\gamma = -\infty$, the action coincides with n : $I = n$, and canonical "angle" variable φ coincides with ϕ . At $\gamma = +\infty$, we have $I = 1 - n$. We are interested in small initial actions, corresponding to the ground state of the quantum system.

We split the initial classical ensemble in slices with equal actions I_- (let us call such an ensemble \mathcal{A}_{I_-}), and analyze dynamics of each slice in detail. Fig.(2) illustrates the algorithm of the analysis. In the infinite past, in variables n, ϕ the slice \mathcal{A}_{I_-} corresponds to a stripe $n = \text{const}, \phi \in [0, 2\pi]$ (see Figs.(2,3)). Initial actions I_- of a classical ensemble in the case of a fully polarized ($\mathbf{n}_- = 0$) initial quantum state are of the order $\frac{1}{N}$ due to quantum fluctuations. In case there is some non-zero initial population of the bosonic mode, I_- can be much larger than $\frac{1}{N}$. There are three small parameters in the model: $\frac{1}{N}$, the sweeping rate ϵ , and the initial action I_- . Naturally, $\frac{1}{N} \ll \epsilon$. Still, freedom of choosing a value of the ratio I_-/ϵ remains. Assuming $I_- \gg \epsilon$ and $\epsilon, 1/N, I_- \ll 1$, which corresponds to considerable initial population of the bosonic mode (see Fig.4), Ref.[13] applied an approach based on the separatrix crossing theory [1, 38, 39]. From the experimental point of view, however, it is important to analyze also cases of very small initial actions.

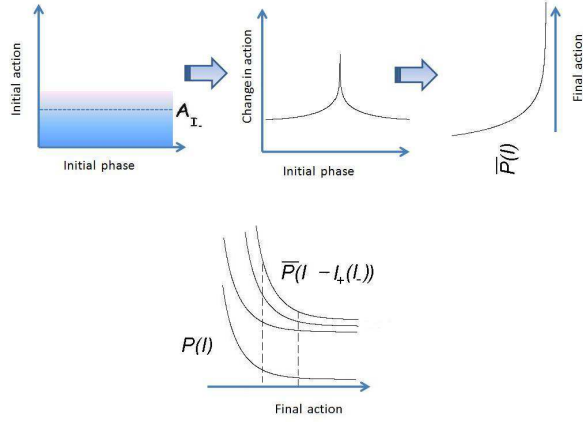


FIG. 2: Build-up of distributions in the action space from the initial Wigner distribution and the change in action during the sweep through the phase transition. This schematic picture applies (with certain modifications) to all three models considered in Sections II-IV. The top left figure illustrates initial distribution $W(I_-) \sim \exp(-NI_-)$, which is exponential in the initial action and uniform in the initial phase. From that distribution, we firstly single out a narrow slice \mathcal{A}_{I_-} of phase points with uniform distribution of initial phases and nearly constant action I_- . As explained in the text, phase points from that slice experience a change in the action $\Delta I(I_-)$ which can be decomposed on the phase independent ($I_+(I_-) \sim \epsilon \ln \pi I_- / \epsilon$) and the phase-dependent ($\mathcal{I}_+(\xi) \sim \ln 2 \sin \pi \xi$) parts (where $\xi \in (0, 1)$ is the pseudophase proportional to the initial phase for the case of small initial actions, as explained in the text). Importantly, the phase-dependent part of the change in the action do not depend on I_- . This phase-dependent part of the change in the action is illustrated in the top center figure. It maps the uniform distribution in the initial phase to a distribution $\bar{P}(I)$ in action space, as illustrated in top right figure. That is, $\bar{P}(I) \sim \frac{1}{\sqrt{4 \exp(\pi I) - 1}}$. Now, to find the overall distribution in action space one needs to integrate over all values of I_- , i.e. to sum up contributions from all \mathcal{A}_{I_-} . As illustrated in the bottom figure, the final distribution is obtained as $P(I) = \int dI_- W(I_-) \bar{P}(I - I_+(I_-))$, see also the corresponding discussion in Section III.

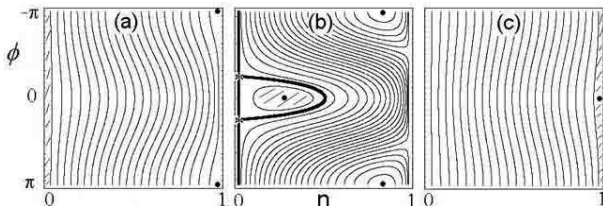


FIG. 3: Phase portraits of (9). From (a) to (c): $\gamma = -10, -1.4, 20$ correspondingly. Saddle points are denoted by asterisks, the bold line is the separatrix. Shaded areas illustrate definitions of the classical actions (see text).

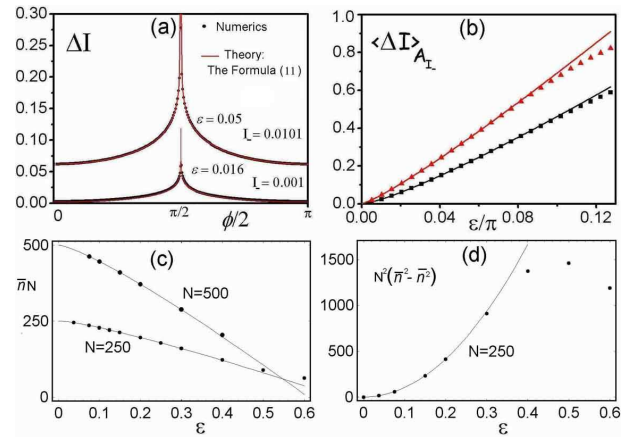


FIG. 4: (a) Change in the action ΔI of classical trajectories from the ensemble \mathcal{A}_{I_-} as a function of the initial phase (Eq.(11)). The change ΔI describes the deviation from adiabaticity. We shift all curves horizontally so that their maxima are at $\pi/2$. We found the change in the action is highly phase-dependent. (b) Average change of the adiabatic invariant $\langle \Delta I \rangle_{\mathcal{A}_{I_-}}$ as a function of the sweep rate ϵ . Lines are the theoretical curves (Eq.(12)). Squares, triangles are numerics for $I_- = 10^{-3}, 10^{-4}$, respectively. (c) Number of created bosons from quantum calculations with $N = 250$ and $N = 500$ (dots); from the Formula (16) obtained by averaging over the initial distribution $W \sim \exp[-2n_b - 2n_\beta]$ (solid lines). (d) Dispersion of the number of bosons for $N=250$; quantum calculations, solid line: the formula (16), i.e. $N^2(\bar{n}^2 - \bar{n}^2) = \frac{N^2 \epsilon^2}{6}$.

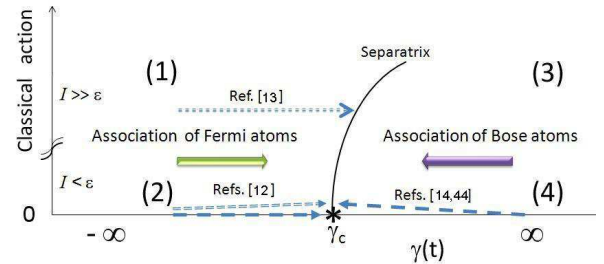


FIG. 5: Regimes of initial conditions and directions of sweeps for a nonlinear LZM Eq.(9). Regimes "1" and "3" correspond to starting far above the classical ground state, where the separatrix crossing theory can be applied [13], which results in Eq.(13). Regimes "2" and "4" can be described by mapping to PII derived here. Starting in the classical ground state in regime 4 (i.e., in "all-atoms" mode in context of bosonic association, or "all-molecules" mode in fermionic association) was considered, e.g., in [14, 44]. A linear power-law with the coefficient $\frac{\ln 2}{\pi}$ was derived in [14]. Starting in the ground state in regime 4, the classical system Eq.(9) always remains in the equilibrium. Taking into account quantum fluctuations of the ground state of Eq.(1) [12] produces an ensemble of initial conditions which leads to Eq.(11).

Our method for the regime of small initial actions is as follows. To calculate the deviation from adiabaticity, we note that most of the change of the classical action of a phase point happens as it travels near the separatrix and, especially, near the saddle points that arise during the bifurcation as γ reaches -2_- [13] (in our new variables, the arising saddle point is located in the origin). Close to the saddle point n is small and one can expand $\sqrt{1-n}$ in series. Let us introduce the variables

$$P = 2\sqrt{n} \cos \frac{\phi}{2}, \quad Y = 2\sqrt{n} \sin \frac{\phi}{2}.$$

Near the bifurcation, at $\gamma \approx -2$, we therefore get an effective Hamiltonian

$$H = -\frac{P^2}{2}(\gamma/2 + 1) - \frac{Y^2}{2}(\gamma/2 - 1) + \frac{P^4}{16},$$

where higher order terms in Y and P have been neglected. We neglect also the time-dependence of the coefficient $\gamma/2 - 1$ of the second term. Then, shifting the origin of time, we obtain the Hamiltonian $-\frac{P^2}{2}\epsilon t + Y^2 + P^4/16$. After simple rescalings $P = 2^{4/3}P'$, $Y = 2^{2/3}Y'$, $t = t'/2^{1/3}$, $H = 2^{7/3}H'$, the Hamiltonian becomes

$$H = -\frac{P^2}{2}\epsilon t + \frac{Y^2}{2} + \frac{P^4}{2}$$

(primes over new variables omitted). We replace also momenta and coordinates: $P \rightarrow Y$, $Y \rightarrow -P$. Let us now introduce a rescaling transformation that makes the essential mathematics of the problem as clear as possible:

$$Y = \epsilon^{1/3}\tilde{Y}, \quad P = \epsilon^{2/3}\tilde{P}, \quad t = \epsilon^{-1/3}s, \quad H = \epsilon^{4/3}\tilde{H}.$$

The Hamiltonian becomes (omitting tildes over new variables)

$$H = -s\frac{Y^2}{2} + \frac{P^2}{2} + \frac{Y^4}{2}.$$

This Hamiltonian does not have a small parameter any more, and the loss of adiabaticity is evident. An important property of the bifurcation we are considering is that the effective Hamiltonian leads to the second Painlevé equation (PII)

$$\frac{d^2Y}{ds^2} = sY - 2Y^3. \quad (10)$$

Asymptotics of PII were investigated by Its and Kapaev [40] (see also [21]) using a method of isomonodromic deformations [41]. At $s \rightarrow -\infty$ the asymptotic solution to (10) is [21, 40]

$$Y(s) = \alpha(-s)^{-\frac{1}{4}} \sin \left(\frac{2}{3}(-s)^{3/2} + \frac{3}{4}\alpha^2 \ln(-s) + \phi \right),$$

and in the limit $s \rightarrow +\infty$ it is

$$Y(s) = \pm \sqrt{\frac{s}{2}} \pm \rho(2s)^{-\frac{1}{4}} \cos \left(\frac{2\sqrt{2}}{3}s^{3/2} - \frac{3}{2}\rho^2 \ln(s) + \theta \right),$$

where (α, ϕ) and (ρ, θ) are the "action-angle" variables characterizing the solutions in the limits $s \rightarrow \pm\infty$. As $s \rightarrow \pm\infty$, the adiabatic invariant I_p of equation (10) approaches the quantities I_p^- or I_p^+ which are defined (to the lowest order terms) as

$$I_p^- = \frac{\alpha^2}{2}, \quad I_p^+ = \frac{\rho^2}{2}.$$

The jump in the adiabatic invariant $\Delta I_p = 2I_p^+ - I_p^-$ can be found from general relations between ρ^2 and α^2 as

$$I_p^+ = \frac{1}{2\pi} \ln \frac{1 + |p|^2}{2|\text{Im}(p)|}, \quad p = \sqrt{e^{2\pi I_p^-} - 1} e^{i[f(I_p^-) - i\phi]}$$

(the function $f(I_p^-)$ is not important for our discussion, see e.g. [14, 21, 40]). Returning back to the original variables and the Hamiltonian (9), we get the Formula:

$$\Delta I = \epsilon \left(\frac{I_-}{\epsilon} - \frac{2}{\pi} \ln \sqrt{\exp \left[\frac{\pi I_-}{\epsilon} \right] - 1} - \frac{2}{\pi} \ln(2 \sin \pi \xi) \right), \quad (11)$$

where for the ensemble \mathcal{A}_{I_-} one has $\pi \xi = (f(I_-) + \frac{\phi}{2})$; ξ is a quasi-random variable uniformly distributed on $(0, 1)$ [42, 43]. The formula predicts the average change in the action to be

$$\langle \Delta I \rangle_{\mathcal{A}_{I_-}} = \epsilon \left(\frac{I_-}{\epsilon} - \frac{2}{\pi} \ln \sqrt{\exp \left[\frac{\pi I_-}{\epsilon} \right] - 1} \right), \quad (12)$$

which means that the final number of bosons (in the ensemble \mathcal{A}_{I_-}) is

$$\bar{n} = 1 - I_- - \langle \Delta I \rangle_{\mathcal{A}_{I_-}}.$$

It predicts also the final distribution $P(\Delta I) = P(1 - I_- - \bar{n})$. All moments $M_{\mathcal{A}_{I_-}}^k \equiv \langle (\Delta I - \langle \Delta I \rangle)^k \rangle_{\mathcal{A}_{I_-}}$ are easy to calculate, for instance

$$M_{\mathcal{A}_{I_-}}^2 = \left(\frac{2\epsilon}{\pi} \right)^2 \int_0^1 d\xi \ln^2(2 \sin \pi \xi) = \frac{\epsilon^2}{3}.$$

Note that the phase-dependent part in (11) exactly coincides with the result of [13], obtained under the different conditions $\epsilon \ll I_- \ll 1$. Moreover, if $I_- \gg \epsilon$, we recover this result of [13], which in the present variables is

$$\Delta I = -\frac{2\epsilon}{\pi} \ln(2 \sin \pi \xi), \quad (13)$$

where the pseudophase $\xi \in (0, 1)$ is a quasi-random variable. Such a change in the action has zero mean value, nevertheless it introduces spreading in particle distribution since $\langle \Delta I^2 \rangle \sim \epsilon^2$. When $I_- \ll \epsilon$, we have a qualitatively different result which resembles that of [12] (i.e. $I_+ = \epsilon \ln I_- / \pi$, with $I_- = \frac{1}{N}$):

$$\Delta I = -\epsilon \left(\frac{1}{\pi} \ln \left(\frac{\pi I_-}{\epsilon} \right) + \frac{2}{\pi} \ln(2 \sin \pi \xi) \right). \quad (14)$$

Formula (11) can be used over a wide range of values of ϵ and I_- (we require $I_- \ll 1$ and $\epsilon |\ln I_-| \lesssim 1$). Qualitatively, it is important that the final distributions are determined not only by the average change in the action (12), but also by the phase-dependent part (13), which is therefore important in *amplification of quantum fluctuations*. The profile of the phase-dependence of ΔI has a striking universality: we found that several other infinitely-coordinated models, e.g. LMG model [23], have analogous behavior during linear sweep of a control parameter through a critical value. The comparison between the numerical and analytical results for $L = 0$ are given in Figs. 4a,b, where predictions of the Eq.(11) start to deviate from the classical numerics only at large ϵ (such that $-\frac{\epsilon}{\pi} \ln \frac{\pi I_-}{\epsilon} \sim 1$).

Now let us remind that the full classical ensemble, governed by the Hamiltonian (8), has distribution of integrals of motion L ; i.e., analysis so far dealt only with a subspace of the initial conditions. To take into account this distribution, we consider slices of the full classical ensemble with equal values of $n + \frac{L}{2} \equiv x$ and uniform distribution of $L \in (-2x, 2x)$; averaging over ϕ and L within the slice, we found that the formula (12) (derived for the "central" point of the slice, i.e. $L = 0, x = I_-$) acquires additional coefficient of 2 inside the logarithm: $I_- \rightarrow 2I_-$. The amplitude of the phase-dependent part is also modified, although it retains its characteristic form shown in Fig. 4a; the final result of averaging over the 3-dimensional distribution (in ϕ, I_-, L) of the initial ensemble of phase points is:

$$\bar{n} = 1 - \frac{\epsilon}{\pi} \left(\ln \frac{\epsilon N}{\pi} + C_\gamma \right), \quad (15)$$

$$\bar{n}^2 - \bar{n}^2 = \frac{\epsilon^2}{6}, \quad (16)$$

where C_γ is the Euler constant. Comparison with numerical quantum calculations are given in Figs. 4c,d.

Let us now briefly discuss the "backward" sweep (see also [14] and Section III), whose properties can also be derived from PII equation. The main feature of the inverse sweep is phase-independence of the change in the action in the limit of small I_- . Deviation from adiabaticity at slow sweeps strictly follows a linear power-law (i.e., phase-dependent terms become negligible). The coefficient of the linear power-law was estimated in [44] to be equal to $\frac{2}{3\pi} \approx 0.21$. The asymptotically exact value of the coefficient was found by us from mapping to PII [14]: $\frac{\ln 2}{\pi} \approx 0.2206$. The most appealing physical system to implement this process is photo- or magneto- association of Bose condensates, which was shown to be well described by a two-mode mean-field model. "Forward" sweep would correspond to dissociation of BEC. Experimentally, studying distributions after a sweep could be achieved by making many runs at each particular sweeping rate.

C. Conclusions

In summary, we have found novel universal features in the dynamics of a many-particle LZM. In particular, the universal profile of Fig. 3a, partly responsible for broad distributions after the sweep, was found. Such universal profiles are very interesting from physical point of view, recall e.g. the Fano profile [45] in AMO physics. There is a classical analogy of the Fano profile (which partly explains its universality): response of two coupled linear oscillators to periodic driving of one of them. Analogously, when an underlying quantum system experiences a *quantum phase transition* (QPT), its classical counterpart experiences a bifurcation. Response of a semiclassical system to slow driving which pushes it through the symmetry-breaking bifurcation, as was shown here, leads to a universal profile $\sim \ln |\sin \pi \xi|$ being imprinted in distributions.

We depicted schematically four different regimes of initial conditions and directions of the sweeps in Fig. 5. It is interesting to compare the expression for the mean number of produced bosons (15) with the results of Refs. [12, 32]. The main difference of our result for the "forward" sweep from Ref. [12] is the coefficient ϵ inside the logarithm of Eq.(15). The model neglects kinetic dispersion of the fermions, but takes into account quantum effects. If we start in the ground state, effectively we have two small parameters: $1/N$ and the sweeping rate ϵ . In the limit of $1/N \rightarrow 0$ the model possess a QPT. At the same time, the model of [32] neglects quantum effects but takes into account fermionic dispersion. It also has two small parameters, the width of a Feshbach resonance γ and dimensionless sweeping rate Γ . In the limit $\gamma \rightarrow 0$ the model of [32] possess a QPT. Our formula Eq.(15) is very close to result of Ref. [32], even though the dynamics is different.

The results reported here are highly relevant for accurately describing the Feshbach resonance passage in ultracold Fermi and Bose gases and may motivate further experimental activity on that theme. Furthermore, we believe our method will have important applications in the field of *dynamics* of QPT [46–49]. An important and interesting direction of the future research would be to extend our method to higher dimensions, i.e. to consider a nonuniform spatially extended system, with coupling of the conversion dynamics to phonon modes, etc.

III. DICKE MODEL WITH CAVITY DECAY AND HIGH FREQUENCY OF THE FIELD MODE: EFFECTIVE LIPKIN-MESHKOV-GLICK MODEL

A. The model

Dicke model with counterrotating terms

$$H = \omega_0 J_z + \bar{\omega} b^\dagger b + \frac{\bar{\lambda}}{\sqrt{2J}} (b^\dagger + b)(J_+ + J_-), \quad (17)$$

considered in detail in the next Section, can be reduced to the Lipkin-Meshkov-Glick model in the limit of high frequency of the field mode $\bar{\omega}$, as shown e.g. in [50]. Consider the Hamiltonian (17) with added dissipation (cavity decay κ), such that $\bar{\omega} \gg \kappa \gg \omega_0$ [50]. Classical equations of motion become

$$\begin{aligned} \dot{x} &= -\omega_0 y \\ \dot{y} &= \omega_0 x - 2\lambda e z \\ \dot{z} &= 2\lambda e y \end{aligned} \quad (18)$$

$$\begin{aligned} \dot{e} &= \bar{\omega} p - \kappa e \\ \dot{p} &= -\bar{\omega} e - 2\lambda x - \kappa p. \end{aligned} \quad (19)$$

The boson field in the corresponding Heisenberg equations of motion can be adiabatically eliminated:

$$b = -\frac{2i\lambda J_x}{(\kappa + i\omega)\sqrt{N}}. \quad (20)$$

which results in the Lipkin-Meshkov-Glick (LMG) model for the spin system [50]

$$H_{LMG} = \omega_0(t) J_z - \frac{\bar{\omega}}{\kappa^2 + \bar{\omega}^2} \frac{(2\lambda)^2}{N} J_x^2 \equiv \omega_0(t) J_z - \frac{\sigma(t)}{N} J_x^2. \quad (21)$$

The LMG model was introduced as a toy model to test the quality of approximations used in multiparticle systems. The structure of the eigenstates of H_{LMG} is compatible with Hartree Fock solutions, therefore one can test, e.g., the validity of Random Phase Approximation against the exact solution. It was also studied recently in the context of dynamics of quantum phase transitions [51–53].

We can study a sweep through a second-order quantum phase transition by changing the coupling $\sigma(t)$, say from 0 to 2, using a smooth pulse that is approximately linear in the vicinity of the critical value of σ , i.e. similar to the previous section. We can choose to change detuning ω_0 instead, thus realizing a clearer analog of the Landau-Zener model (also, the problem becomes analogous to that studied in [51]). The system is very much related to that studied in Section II, but now the dynamics of almost all classical trajectories are captured by PII

and we can study quantum-classical correspondence in a greater detail.

After the rescalings $H \rightarrow H/\sigma, t \rightarrow t/\sigma$ Hamiltonian can be brought to the form

$$H = -\gamma(t) J_z - \frac{1}{N} J_x^2, \quad (22)$$

where $\gamma = \frac{\omega_0}{\sigma} = \epsilon t$. In the basis of $\{|j\rangle \equiv |\frac{N}{2}, 2j-2-\frac{N}{2}\rangle\}$, the matrix elements have the form

$$\begin{aligned} H_{j,j} &= 1 - j + \frac{2}{N}(j-1)^2 - \gamma(-N/2 - 2 + 2j), \\ H_{j,j+1} &= -\frac{1}{4N} \sqrt{2j(2j-1)(N+1-2j)(N+2-2j)}. \end{aligned} \quad (23)$$

The energy levels are depicted on Fig.(6)a. Fig.(6)b shows the locations of the branch points in the complex γ -plane. At extremely slow sweeps, in the lowest order of the sweeping rate the probability of transition from $i-th$ to $j-th$ eigenstate is determined by the Dykhne formula [54] and depends on the integral around the branch point connecting $i-th$ and $j-th$ eigenvalues $E_{i,j}(\gamma)$. The regular structure seen in the picture suggests that there is a universality in the distribution of probabilities in this (extremely slow) regime, the analysis of which we postpone for future research. Here we concentrate on a faster, semiclassical regime.

B. Classical ensembles and quantum dynamics

Classical limit of the LMG model is obtained, as above, from the Heisenberg equations, and is given by

$$H = -\gamma z - \frac{1-z^2}{4}(1 + \cos 2\phi), \quad (24)$$

where $z \in [-1, 1]$ is the dimensionless counterpart of J_z , and $\phi \in [-\pi, \pi]$ is the canonically conjugated phase.

The initial distribution of z following from SU(2) Wigner function is exponential for large N : $P(z) \approx N \exp[-(1+z)N]$. For large negative λ , the classical ground state is at $z = -1$; at $\gamma = -1$ a bifurcation occurs. For $\gamma \in (-1, 1)$ the stable fixed points (s.f.p.) are at $z = \gamma, \phi = 0, \pi$. Phase portraits are shown in Fig.(7). It is easy to demonstrate that a passage through bifurcation at $\gamma = -1$ is similar to that happening in the Hamiltonian system (8) with $L = 0$, studied in Section II. Moreover, we do not have complications arising from $L \neq 0$ initial conditions anymore. Also, a passage through the bifurcation at $\gamma = 1$ happening with increasing γ is analogous to the "inverse" sweep mentioned in Section II. We consider several scenarios below.

Consider firstly a scenario where $\gamma(t)$ is changed from a large negative value to zero. The quantum system in the end of the sweep is described by the Kerr Hamiltonian $-S_x^2$ [55]. In the short-time evolution after the

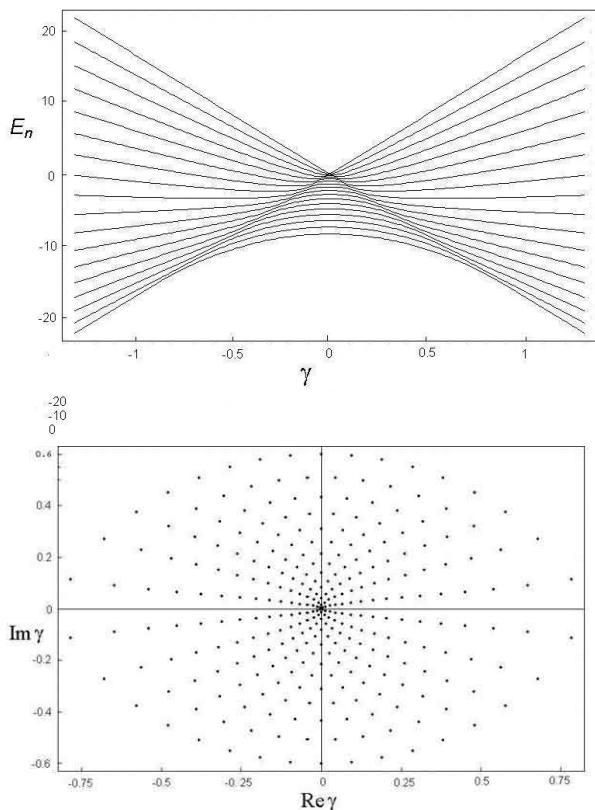


FIG. 6: Energy levels of the LMG model $E_n(\gamma)$ (upper panel) and its branch points in the plane of complex γ (bottom panel).

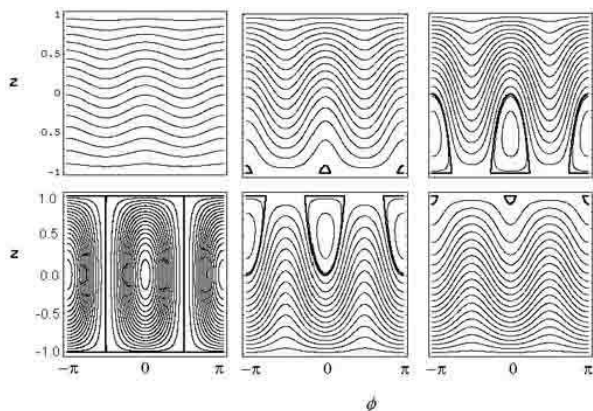


FIG. 7: Phase portraits of the LMG Hamiltonian at $\gamma = -3, -0.5, -0.95$ (from left to right in the upper panel) and $\gamma = 0, 0.5, 0.95$ (from left to right in the bottom panel). Note that bifurcations happen at $\gamma = \pm 1$.

sweep, both semiclassical and quantum systems exhibit damped oscillations of $\langle J_z \rangle$. Damping comes from dephasing of the TWA classical trajectories in the anharmonic effective potential. In the process of dephasing, $\langle J_z \rangle$ exhibits decaying oscillations around its mean (time-averaged) value which we denote $\overline{\langle J_z \rangle}$.

As a signature of nonadiabaticity, let us consider the

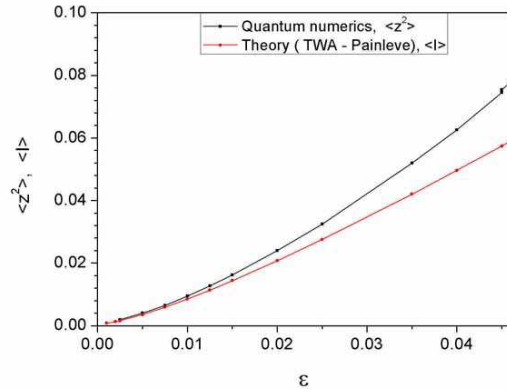


FIG. 8: Comparison of the dispersion of J_z in a quantum system $\sigma(J_z) = (\overline{\langle J_z^2 \rangle} - \overline{\langle J_z \rangle}^2)/(N/2)^2 \approx \overline{\langle J_z^2 \rangle}/(N/2)^2$ and the classical prediction from the mean change in classical action of the TWA ensemble, $\langle I \rangle$ (Eq. 25).

time-averaged dispersion of $\langle J_z \rangle(t)$, or the mean value of the second moment $\overline{\langle J_z^2 \rangle}$ around which the dispersion of $\langle J_z \rangle(t)$ oscillates. In the classical system, at the final value $\gamma = 0$, the Hamiltonian linearized around its s.f.p. $\{z = 0, \phi = 0\}$ is $H = \frac{z^2}{2} + \frac{\phi^2}{2}$. Therefore the dispersion of z is related to the mean value of the classical action in the first approximation. That is, assuming a uniform distribution of the final phase of trajectories of the classical wavepacket (i.e., after dephasing), one obtains

$$\begin{aligned} \overline{\langle z^2 \rangle} &= \overline{\langle I \rangle} \\ &\approx \int_0^\infty \left[\frac{3(1+z_0)}{4} - \frac{\epsilon}{\pi} \ln \left(\frac{\pi(1+z_0)}{2\epsilon} \right) \right] N e^{-(1+z_0)N} dz_0 \\ &= \frac{3}{4N} + \frac{\epsilon}{\pi} \left(C_\gamma + \ln \left(\frac{2\epsilon N}{\pi} \right) \right) \\ &\approx \frac{\epsilon}{\pi} \left[C_\gamma + \ln \left(\frac{2\epsilon N}{\pi} \right) \right], \end{aligned} \quad (25)$$

where $C_\gamma \approx 0.577$ is the Euler constant. Here, $\langle \dots \rangle$ denotes averaging over the ensemble, while overline denotes time-averaging. Dispersion of $\langle J_z \rangle$ in a quantum system with $N = 1024$ is compared with Eq.(25) in Fig. 8. One can see a remarkable coincidence of the theoretical predictions and numerics at slow sweeps. Deviations at fast sweeps are due to inapplicability of the Painleve mapping. We note a universality of the obtained formula: the equivalent linear plus linear-logarithmic law was derived in Section II.

Let us consider the semiclassical distribution in action space after the sweep. In Section II we already derived the distribution $\tilde{P}(I)$ coming from the phase-dependent part of change in the action. We consider now in detail how it is summed up to the full distribution.

Let us work with the rescaled action $\tilde{I} = \frac{I}{4\epsilon}$, where I is the action of the Hamiltonian (24).

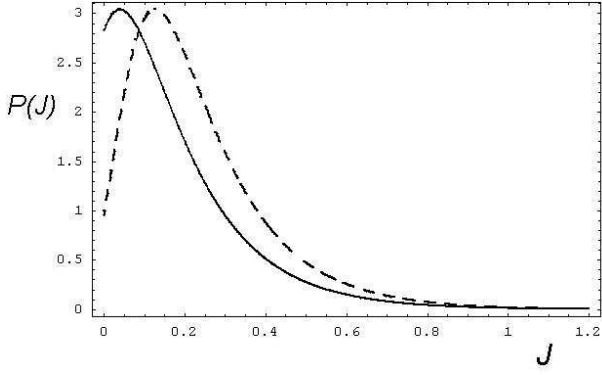


FIG. 9: The distribution $\text{cal}P(\tilde{J})$ in the rescaled action space after the sweep, Eq. (30). Solid line: $\epsilon = 0.015$. Dashed line: $\epsilon = 0.005$.

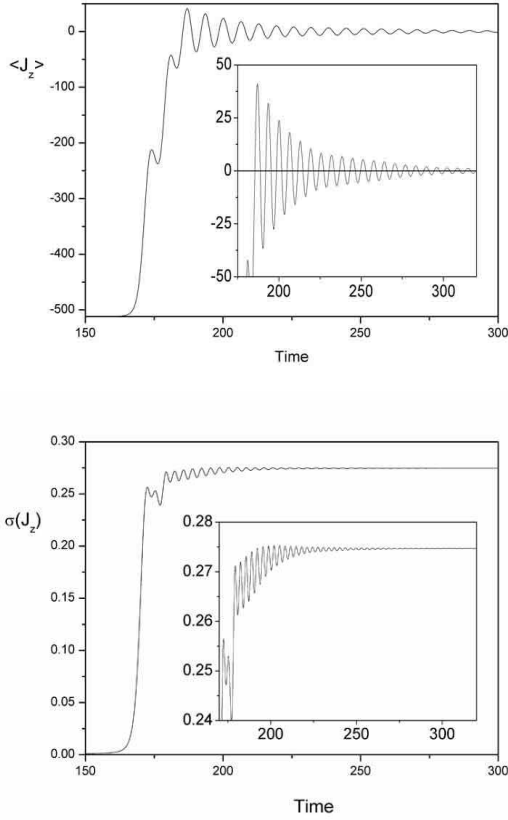


FIG. 10: Dynamics of J_z (upper panel) and the dispersion of J_z (bottom panel) in the quantum system, $N=1024$, $\epsilon = 0.045$.

Following the analysis of Section II, action after the sweep through the critical $\gamma = -1$ (\tilde{I}_+) is related to the initial rescaled action \tilde{I}_- as

$$\tilde{I}_+ = \tilde{I}_- - \frac{1}{2\pi} \ln \sqrt{\exp(2\pi\tilde{I}_-) - 1} - \frac{1}{2\pi} \ln 2 \sin \pi\xi'. \quad (26)$$

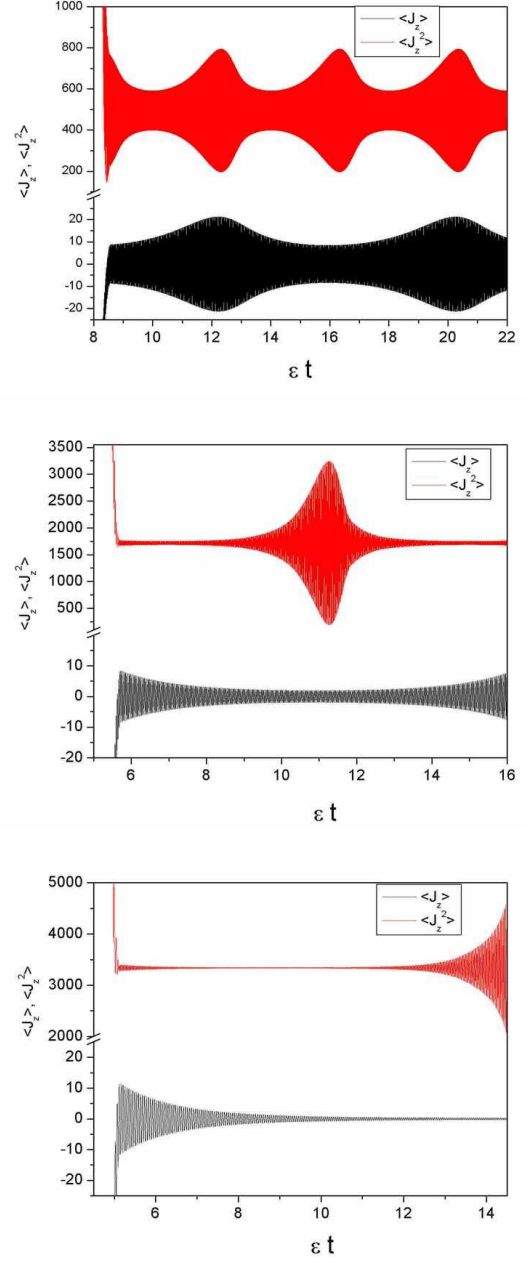


FIG. 11: Dynamics of $\langle J_z \rangle, \langle J_z^2 \rangle$ for $\epsilon = 0.0025, 0.005, 0.0075$ (from top to bottom) in the quantum system, $N=1024$. Note the different scales in each figure for $\langle J_z \rangle$ and $\langle J_z^2 \rangle$. The time scales in both figures look shifted because we use smooth turn-on and turn-off of sweeping of the parameters. Both magnitudes after the sweep undergo oscillations around its time-averaged values, $\overline{\langle J_z \rangle}$ and $\overline{\langle J_z^2 \rangle}$, correspondingly (overline denotes time-averaging here, while $\langle \dots \rangle$ denotes instantaneous mean value of an operator, i.e. averaging over the state). It can be seen that $\overline{\langle J_z \rangle} = 0$, while $\overline{\langle J_z^2 \rangle}$ is a function of the sweeping rate ϵ , as shown in Fig. (8).

Let us consider firstly the phase-dependent part of change in the action $-\frac{1}{2\pi} \ln 2 \sin \pi \xi$. It leads to the distribution

$$\bar{\mathcal{P}}(\tilde{I}_f) = \frac{2}{\sqrt{4 \exp(4\pi \tilde{I}_f) - 1}} \quad (27)$$

in the final action space. Additionally, each slice $\mathcal{A}_{\tilde{I}_-}$ gets a different phase-independent change

$$\tilde{I}_+(\tilde{I}_-) = \tilde{I}_- - \frac{1}{2\pi} \ln \sqrt{\exp(2\pi \tilde{I}_-) - 1} \approx \frac{3}{4} \tilde{I}_- - \frac{1}{4\pi} \ln 2\pi \tilde{I}_-. \quad (28)$$

The final distribution is

$$\mathcal{P}(\tilde{I}) = \int \bar{\mathcal{P}}(\tilde{I} - \tilde{I}_+(x)) W(x) dx, \quad (29)$$

i.e., it is an integral of the distribution $\bar{\mathcal{P}}(\tilde{I} - \tilde{I}_+(\tilde{I}_-))$ originating from a phase-dependent change in action $\bar{\mathcal{P}}(\tilde{I})$ of an ensemble $\mathcal{A}_{\tilde{I}_-}$ shifted by value of phase-independent change in action of that ensemble over the initial exponential distribution of initial actions $W(\tilde{I}_-) = N \exp[-\tilde{I}_- N]$. After simple manipulations, neglecting the term $\frac{3}{4} \tilde{I}_-$ in (28), we get

$$\mathcal{P}(\tilde{I}) = \sqrt{8\epsilon N} \exp(-2\pi \tilde{I}) \exp\left(-\frac{\epsilon N}{2\pi} \exp[-4\pi \tilde{I}]\right), \quad (30)$$

see Fig. 9.

It is easy to see that normalization of the distribution (30) is less than 1: the total probability is $\int P(I) dI = \text{Erf} \sqrt{\frac{\epsilon N}{2\pi}}$, which is close to 1 only for $\epsilon N \gg 1$. This discrepancy is due to the approximations in (28), which were necessary to obtain the analytical expression (30). Nevertheless, even at $\epsilon N \sim 1$ the obtained analytical formula correctly describes distributions at small final actions $I_f \ll 1$. We believe that $P(I_f)$ may be fitted to the Gumbel distribution as done in [12].

The distribution is manifested, in particular, in the final dispersion of $\langle J_z \rangle$. Indeed, for a Morse oscillator $H = -\frac{1}{2}(1 - I)^2$ a trajectory with $I = \text{const}$ has $z^2(t) = \frac{1 - (1 - I)^2}{2} = (I - \frac{I^2}{2})$. The dispersion of z of the whole wavepacket is therefore

$$\bar{z}^2 = \int (I - \frac{I^2}{2}) \mathcal{P}(I) dI = \bar{I} - \frac{\bar{I}^2}{2}. \quad (31)$$

This formula shows that anharmonicity of the final Hamiltonian provides an additional means of measuring the final phase-space distribution. Indeed, now the dispersion of z depends not only on the mean value of I , but also on its second moment. The additional contribution from anharmonicity is given by

$$\begin{aligned} \delta z^2 = & -\frac{2}{3} \frac{\epsilon^2}{\pi^2} \left(\pi^2 \right. \\ & \left. + 6(C_\gamma + \ln N)^2 + 6 \ln \left(\frac{2\pi}{\epsilon N^2} - 2C_\gamma \right) \right) \ln \left(\frac{2\pi}{\epsilon} \right). \end{aligned}$$

Having obtained the distribution (30) resulting from "forward" sweep through the QPT, it is interesting to find out what happens with this distribution if γ is slowly swept back, and the system is pushed through the QPT in "backward" direction. Alternatively, one may choose not to stop a sweeping of γ at $\gamma = 0$, but continue to change it (linearly in time) beyond the next critical point $\gamma = 1$.

So, we consider the second possible scenario which involves a sweep from $\gamma = -\infty$ to $\gamma = +\infty$. Then, the system undergoes a passage through a bifurcation twice: at $\gamma = -1$ and at $\gamma = 1$. The latter passage has a very different behaviour: in particular, the jump in the classical action of a trajectory is phase-independent for small values of initial actions, like in the backward sweep of the model of Section II.

The adiabatic invariant after the inverse sweep \tilde{I}_{++} is given by the following formula [21]:

$$\tilde{I}_{++} = \frac{1}{2\pi} \ln(1 + |p|^2), \quad (32)$$

where

$$p = p_r + p_i, \quad p_r = \text{sign}(\sin c) \sqrt{(1 - b^2)(a^2 - 1)}, \quad (33)$$

$$p_i = a - b\sqrt{a^2 - 1}, \quad b = \cos c, \quad (33)$$

$$c = \phi + \tilde{f}(I_+), \quad a = \exp(2\pi I_+), \quad (34)$$

where $\tilde{f}(I_+)$ is a function of I_+ ; I_+ denotes the value of the adiabatic invariant after a direct sweep and before the inverse sweep, say at $\gamma = 0$. We assume that dephasing of phase points happening between the first and the second passage through bifurcations lead to uniform distribution of the magnitude of c . Denote as $\langle I_{++} \rangle_c$ the mean value of I_{++} averaged over the initial phase c . Since

$$I_{++} = \frac{1}{2\pi} \ln(2a^2 - 2ab\sqrt{a^2 - 1}), \quad (35)$$

we get after averaging over c :

$$\langle I_{++} \rangle_c = \frac{1}{2\pi} \ln(a^2 + a). \quad (36)$$

The average over the whole ensemble is achieved now by averaging over the distribution of actions $\mathcal{P}(I_+)$:

$$\langle I_{++} \rangle = \frac{1}{2\pi} \int dI_+ \ln(a^2 + a) \mathcal{P}(I_+). \quad (37)$$

Therefore, the distribution $\mathcal{P}(I_+)$ before the second bifurcation passage leads to the following prediction for the final values of $\langle J_z \rangle$:

$$\begin{aligned} \overline{\langle J_z \rangle} = & 2\epsilon N \int_0^\infty dI \sqrt{8\epsilon N} \exp[-2\pi I] \times \\ & \times \exp\left[-\epsilon N \frac{\exp[-2\pi I]}{2\pi}\right] \frac{\ln(\exp(2\pi I) + \exp(4\pi I))}{2\pi}. \end{aligned} \quad (38)$$

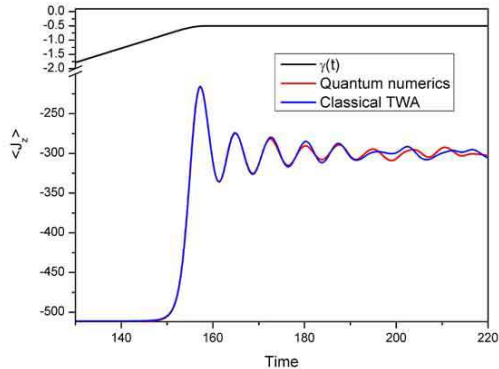


FIG. 12: Sweeping from $\gamma = -8$ to $\gamma = -0.5$. The system undergoes a phase transition at $\gamma = -1$ and the sweeping is stopped at $\gamma = -0.5$. Short-time evolution exhibits remarkable coincidence of quantum and semiclassical dynamics. $\epsilon = 0.05$, $N = 1024$.

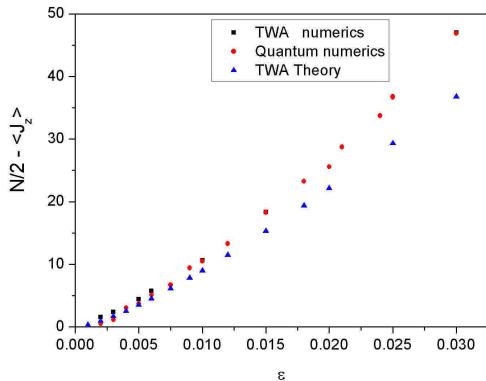


FIG. 13: Sweeping from $\gamma = -8$ to $\gamma = 16$. The system undergoes two consequential phase transitions at $\gamma = \mp 1$. The final values of $\langle J_z \rangle$ are shown, extracted from quantum numerics, classical TWA numerics, and TWA-Painleve theoretical prediction. Theoretical TWA prediction (Eq.(38)) is depicted as triangles; circles: quantum numerics, and TWA numerics is shown by squares. We note that up to $\epsilon \geq 0.1$ TWA numerics closely reproduce quantum numerics, however slightly deviate from TWA theoretical prediction (38). Also, at very slow sweeps $\epsilon \leq \frac{1}{N}$ deviations between TWA and quantum numerics can be seen.

The correspondence between theoretical prediction, quantum numerics and TWA numerics is shown in Fig.13.

We note that up to $\epsilon \geq 0.1$ TWA numerics closely reproduce quantum numerics, but starts to considerably deviate from TWA theoretical prediction at $\epsilon \sim 0.1$. the assumption of uniform phase distribution before the second bifurcation passage seems to be not fulfilled here. Also, at $\epsilon \leq \frac{1}{N}$ deviations between TWA and quantum numerics can be seen which can be attributed to finite-size corrections and interference effects.

IV. DICKE MODEL WITH COUNTERROTATING TERMS

A. The model

For many applications, counterrotating terms should be included in the model Hamiltonian:

$$H = \omega_0 J_z + \bar{\omega} b^\dagger b + \frac{\bar{\lambda}}{\sqrt{2J}} (b^\dagger + b)(J_+ + J_-), \quad (39)$$

here the angular momentum operators describe an ensemble of two-level systems of level-splitting ω_0 in terms of a collective spin of length $J = N/2$. The field mode frequency is $\bar{\omega}$. A physical realization is e.g. an ensemble of two-level atoms in a cavity; ground state of such a system corresponds to the absence of photons (field vacuum) and complete angular momentum inversion ($J_z = -N/2$, all atoms in the lowest state).

We introduce a rescaled coupling $\lambda = \bar{\lambda}/\omega_0$, a dimensionless frequency $\omega = \bar{\omega}/\omega_0$, and a dimensionless time $t' = \omega_0 t$. The Hamiltonian now depends on two parameters

$$H = J_z + \omega b^\dagger b + \frac{\lambda}{\sqrt{N}} (b^\dagger + b)(J_+ + J_-). \quad (40)$$

There are several different approaches to obtain semiclassical equations of motion: through coherent states [56], Holstein-Primakoff transformation [27], and from Heisenberg equations of motion through straightforward c-number formalism [57]. We choose to use the latter approach, but with a very important additional detail: we combine it with the Wigner function approach of Altland et al. [12]. That is, we firstly investigate classical equations of motion analogous to that of [57], for the case of sweeping the coupling through the quantum phase transition. Then, we prepare an ensemble of classical trajectories corresponding to our initial quantum state (field vacuum and complete angular momentum inversion, $J_z = -N/2$), and compare quantum and classical dynamics. The magnitude of any quantum observable is obtained by averaging over the classical ensemble.

B. Classical dynamics

Similar to the case of Eq.(3) in Section II, classical dynamics is obtained from Heisenberg equations of motion and is described by five dynamical variables:

$$\begin{aligned} \dot{x} &= -y \\ \dot{y} &= x - 2\lambda e z \\ \dot{z} &= 2\lambda e y \\ \dot{e} &= \omega p \\ \dot{p} &= -\omega e - 2\lambda x. \end{aligned} \quad (41)$$

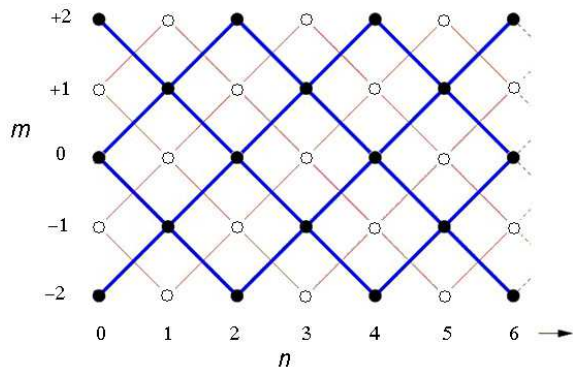


FIG. 14: The Hilbert space of the Dicke model, for $2j = N = 2$. m is the z -projection of angular momentum, J_z ; n is number of photons; see also [27].

The integrals of motion are $r = x^2 + y^2 + z^2 = 1$ (irrespective of the time-dependence of the parameter λ) and $\frac{W}{2} = z + \frac{\omega}{2}(e^2 + p^2) + 2\lambda ex$ (only at constant λ).

As the classical system has two degrees of freedom and is not integrable, its phase space is generally not regular. Some issues of chaotic dynamics in Dicke model with counterrotating terms were discussed, e.g., in [57]. At small values of coupling λ , and small detunings (i.e., $\omega \approx 1$) the classical phase space is mostly regular, with a small chaotic layer around the separatrix of the unperturbed ($\lambda = 0$) problem. As the value of the coupling is increased, the chaotic region of the phase space also grows, and near the critical coupling "global" chaos sets in.

It is interesting to note that in our case, for a passage through the critical point, chaos is not relevant. Dynamics in a vicinity of the stable fixed point is regular. In the critical region, classical trajectories do diverge from each other, however this dynamics is captured by the Painleve equation. After passing the critical region, dynamics is again confined in the regular regions of the phase space (provided the sweep was not too fast). A passage through the critical region can be analyzed in a similar way to the models of Section II and III.

Introducing pairs of canonically conjugated variables (z, θ) , (I, ϕ) as

$$\begin{aligned} x &= \sqrt{1 - z^2} \cos \theta \\ y &= \sqrt{1 - z^2} \sin \theta \\ p &= \sqrt{2I} \cos \phi \\ e &= \sqrt{2I} \sin \phi, \end{aligned} \quad (42)$$

we get a Hamiltonian with two degrees of freedom

$$H = \frac{W}{2} = z + \omega I + 2\lambda \sqrt{2I(1 - z^2)} \cos \theta \sin \phi. \quad (43)$$

At $\lambda = 0$, dynamics is (obviously) integrable, and the system possesses two classical actions: $I_1 = I$, $I_2 =$

$1 + z$. In a fully classical approach, the initial state at $\lambda = 0$ would be the equilibrium $z = -1$, $I = 0$, i.e. $I_{1,2} = 0$. Sweeping the value of λ , the system would stuck in this equilibrium even when it becomes unstable at λ larger than critical. In the TWA semiclassical approach, an ensemble of phase points with initial actions $I_{1,2} \sim \frac{1}{N}$ should be considered. As a result of sweeping λ through the phase transition, both actions undergo changes which depend on the sweeping rate ϵ . Provided the parameter $\epsilon / \ln N$ is not too large (i.e., the sweep is not too fast, or the number N is large enough), the final dynamics will take place in the *regular* region of the phase space, as shown below. In this region, it is possible to introduce two classical actions which depend on initial ones and the sweeping rate. Thus, short-time dynamics after the passage through the quantum phase transition can be studied using classical adiabatic theory.

To study the dynamics of the phase transition, we need to obtain an effective Hamiltonian in the vicinity of the critical region. We do it through the set of canonical transformations described in the Appendix C. They bring us to the Hamiltonian

$$H = 32(P_1^2 + Q_1^2) + \frac{P^2}{2} + \frac{Q^4}{2} - \epsilon t \frac{Q^2}{2}. \quad (44)$$

In the lowest order approximation, the adiabatic invariant associated with the first pair of variables P_1, Q_1 is conserved, while that associated with another pair of variables P, Q experiences a jump according to PII.

After calculating this jump (which is equivalent to that found in previous Section), we consider "final" dynamics at couplings stronger than the critical. There exists several possible regimes of motion. Figures 15-17 demonstrate, in particular, three distinct regimes of the dynamics after the sweep. If the final coupling is far away from the critical (Fig.15), effective Hamiltonian is that of two weakly coupled harmonic oscillators. One can see that the photon number undergoes harmonic oscillations with almost constant amplitude, which can be taken as a quantitative measure of the nonadiabaticity. On the other hand, if the final coupling is close to the critical one, while the sweeping rate is considerably high, one can observe rapid deviation between TWA and quantum dynamics due to interference terms not accounted for by the TWA method in the lowest order approximation. Trajectories entering chaotic regions of the phase space also make semiclassical dynamics complicated. However, an interesting and important regime of motion happens in case the final coupling is not far away from the critical one (such that the expansions mentioned above remain valid), while the sweeping rate is sufficiently slow to leave most of the classical wavepacket in the regular region of the phase space (Fig.17). Then, a phase point acquires a classical actions I_2 by the time the pulse $\lambda(t)$ is accomplished and keeps the classical action I_1 to be almost zero ($I_{1,2}$ are now related, correspondingly, to local variables (q_1, p_1) and (q_2, p_2) introduced in the Appendix C rather than to z and I as above). Considerable magnitude of

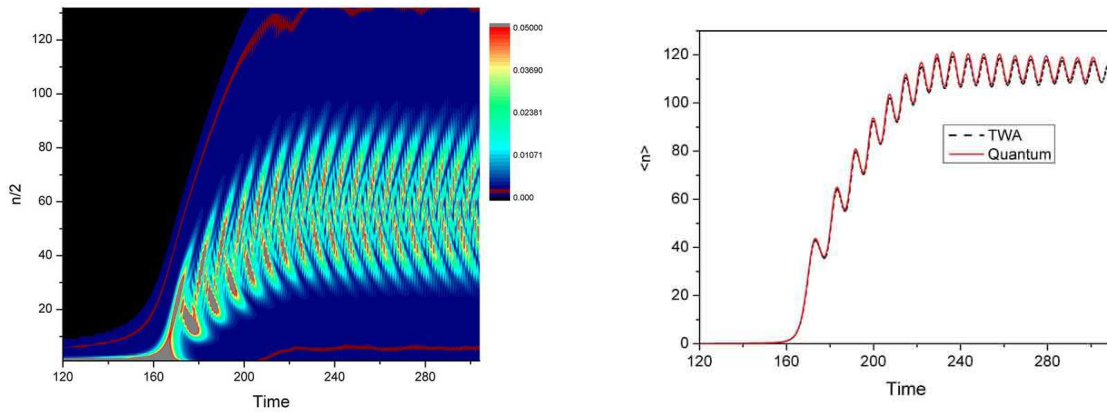


FIG. 15: Time evolution of the photon distribution in quantum numerics (left), and the mean photon number in quantum and TWA numerics (right) for a sweep from $\lambda = 0.25$ to $\lambda = 0.75$ in the Dicke model on resonance $\omega = 1$. The parameters are $\epsilon = 0.01, N = 250$. The correspondence between semiclassical TWA and quantum calculations is nearly perfect.

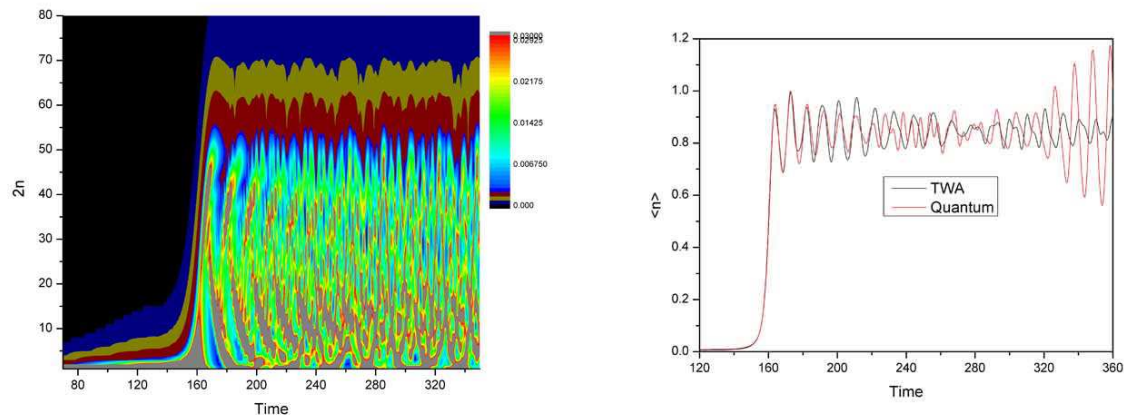


FIG. 16: Time evolution of the photon distribution in quantum numerics (left), and the mean photon number in quantum and TWA numerics (right) for a sweep from $\lambda = 0.45$ to $\lambda = 0.55$ in the Dicke model with large difference of frequencies $\omega = 50$. The parameters are $N = 500, \epsilon = 0.04$. The correspondence between semiclassical TWA and quantum calculations degrades with time.

I_2 leads to effective dephasing between different trajectories, as seen in Fig.17 (effective final Hamiltonian is not linear). As a result the photon number undergoes *damped* oscillations around certain mean value. We consider this regime in detail. As a signature of nonadiabaticity, we take the mean (time-averaged) value of amplitude of oscillations of number of photons. Faster sweeps lead to a shift of this value downwards (see Fig.17). As shown in Appendix C, in close analogy with Section III, after averaging over the initial TWA distribution one has

$$\langle \bar{n} \rangle \approx 4\delta\lambda_f - \frac{\langle I \rangle}{4\sqrt{\delta\lambda_f}}, \quad (45)$$

where the final coupling is $\lambda_f = \frac{1}{2} + \delta\lambda_f$ and the mean action of trajectories of the classical wavepacket is

$$\langle I \rangle = \frac{3}{4N} + \frac{8\sqrt{2}\epsilon}{\pi} \left(C_\gamma + \ln \left(\frac{2N\epsilon 8\sqrt{2}}{\pi} \right) \right). \quad (46)$$

This prediction is compared with TWA numerics for $N = 500$ and $\delta\lambda_f = 0.03$ in Fig.17. Remarkable coincidence can be seen at relatively slow sweeps.

V. CONCLUSIONS

We provided a method to treat the dynamics of quantum phase transitions in systems whose classical counterparts have a few degrees of freedom. The initial state of a quantum system (which is chosen to be close to its ground state) is represented by an ensemble of classical phase points initially concentrated in a $\frac{1}{N}$ -vicinity of a stable fixed point. By sweeping a parameter, the quantum system is transferred through a quantum phase transition, which in the underlying classical system corresponds to a bifurcation. Second-order QPT usually corresponds to a pitchfork bifurcation, while first-order QPT to saddle-centre bifurcation. Magnitudes of quantum observables

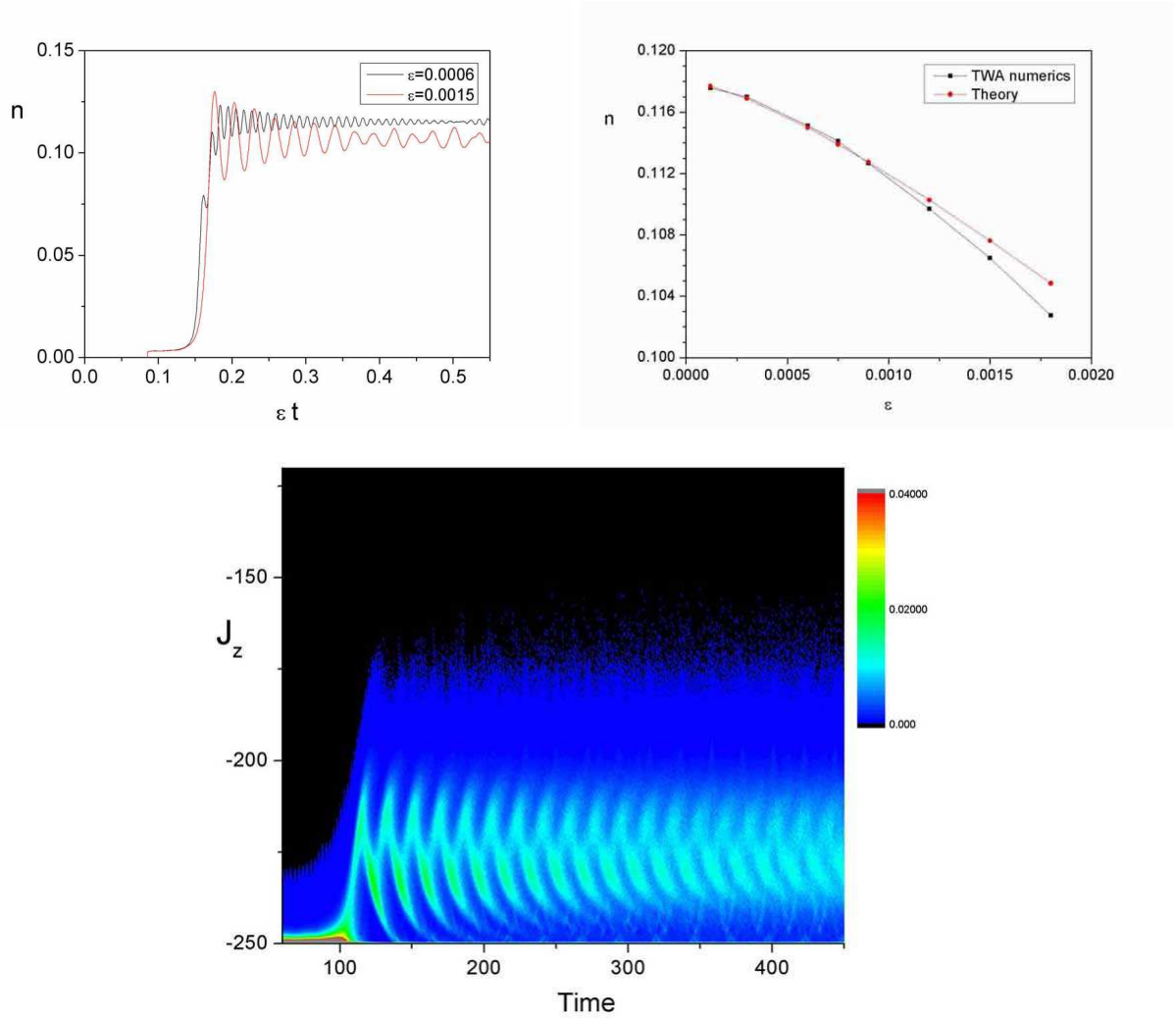


FIG. 17: Sweep through the critical coupling from $\lambda = 0.47$ to $\lambda_f = 0.53$, $\omega = 1$, $N = 500$. TWA numerics and theoretical TWA-Painleve prediction is given. Top left: time evolution of the photon number for different sweeping rates. The photon number undergoes damped (due to semiclassical dephasing) oscillations around a mean value. Faster sweeps lead to shift of the mean value downwards and increase of the initial amplitude of these oscillations. Top right: the mean value (i.e., time-averaged value) of the photon number after the sweep for different sweeping rates, comparison of the TWA numerics and the theoretical prediction (Eqs.(45,46)). Bottom: dynamics of distribution of J_z during the sweep in TWA numerics (similar dynamics for the photon distribution).

are obtained by averaging over the classical distribution. From the properties of the Wigner function it follows that the initial angle of the phase points in the ensemble (i.e., the phase canonically conjugated to an action variable) is uniformly distributed on $(0, 2\pi)$. As a result of the passage through a bifurcation, the canonical action undergoes a phase-dependent jump. As a function of the sweeping rate and initial action, this jump for a pitchfork bifurcation has very peculiar properties.

A central idea of the method is as follows: far from the bifurcation, classical actions are approximately conserved (due to adiabatic invariance of action). In the vicinity of a bifurcation, the system can be brought to a "normal" form: the first Painleve equation for the saddle-center bifurcation, and the second Painleve equation for

the pitchfork bifurcation. Change in the action is determined by these effective equations. The method provides an asymptotically exact theory, i.e. coefficients of the power-laws derived, etc., are asymptotically *exact*. To be specific, we considered here several particular models: Dicke models with and without counterrotating terms, and the Lipkin-Meshkov-Glick model.

The results are as follows.

(i) The most important results for the Dicke model without counterrotating terms: (i) the linear-logarithmic power-law for the forward sweep, and the linear power-law with the coefficient $\frac{\ln 2}{\pi}$ for the inverse sweep. Properties of the initial Wigner distribution are such that additional trajectories not described by the PII equation appear, which modify the coefficients of the power-law in

the forward sweep.

(ii) The most important results for the Dicke model with counterrotating terms are as follows. Even though it is usually assumed that superradiant phase corresponds to chaotic classical dynamics, i.e. the bifurcation at critical coupling leads to chaotic phase space, we found that close to the new equilibria (emerging in the superradiant phase) phase space is regular; it is possible to introduce two classical actions there. Now, in the limit of large N initial classical wavepacket is highly localized near the equilibrium; therefore at not very fast sweeps it will remain in the regular area of the phase space after the sweep. One may ask what changes in the classical actions will be. We found the dynamics of passage through bifurcation happens in the way where, although there are two pairs of canonical variables those frequencies are of the same order far from bifurcation, in the vicinity of the bifurcation a separation of time-scales happens and by a suitable transformation it is possible to define a pair of (slow) variables those dynamics is described by PII and another pair of (fast) variables which conserves its classical action. Briefly, passage through the bifurcation in the multidimensional system happens effectively in a 'one-dimensional' way.

(iii) The Dicke model with large discrepancy of frequencies and large dissipation, relevant to the [25] experiment, can be approximated by the LMG model [50]. The passage through a bifurcation there is also described by PII. What is exciting in this model is that all trajectories from the initial distribution are described by PII.

An important question is how to detect the final distributions experimentally. While in the model of Section II one can directly measure the final distributions of number of molecules, in the case of LMG model (Section III) and sweep to $\gamma = 0$ the situation is more complicated. A possible scenario would involve measuring the time-averaged dispersion of J_z after the sweep, which will depend on the distribution of the final action due to the nonlinearity of the effective Morse oscillator. In the case of Model of Section IV one can monitor (for instance) a shift in the time-averaged value of the photon number as a function of the sweeping rate.

Acknowledgements

This work was supported by the Academy of Finland (Projects No. 213362, No. 217043, and No. 210953) and EuroQUAM/FerMix, and conducted as a part of a EURYI scheme grant (see www.esf.org/euryi). A.P.I. was partly supported by RFBR 09-01-00333. We are grateful to A.I. Neishtadt, A.Polkovnikov, V.Gurarie, A.B.Klimov, L.Plimak for illuminating discussions.

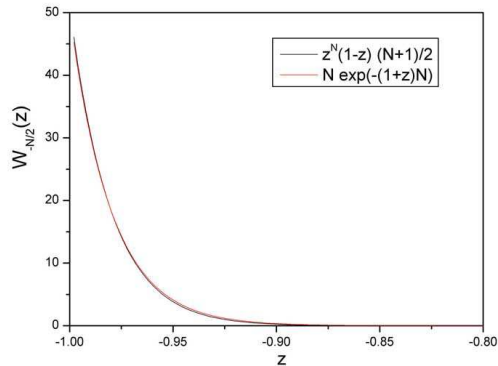


FIG. 18: The Wigner function of the state $|\frac{N}{2}, -\frac{N}{2}\rangle$. Here we compare two functions approximating the exact $SU(2)$ Wigner function, $z^N(1-z)^{\frac{(N+1)}{2}}$, and $N \exp[-(1+z)N]$, for $N = 50$. Note that the two curves are almost indistinguishable on that scale.

Appendix A: Wigner function distributions

Very useful approximate expressions for $SU(2)$ Wigner functions of J_z operator eigenstates were obtained in [16, 17]. In the limit of large dimension of representation $J \gg 1$, result of [17] for J_z eigenstate $|k, J\rangle$ is

$$W_k(\theta, \phi) \approx (-1)^{J+k} d_{kk}^J(2\theta) \left[1 + \frac{k}{J} \cos \theta\right] \frac{N+1}{2}, \quad (47)$$

where d_{kk}^J is the (small) Wigner d-function, which is related to Jacobi polynomials.

For the ground state $k = -J = -\frac{N}{2}$ one gets

$$\begin{aligned} W_{-J}(\theta, \phi) &= d_{-J, -J}^J(2\theta) \left[1 - \cos \theta\right] \frac{N+1}{2} \\ &= (\cos \theta)^{2J} \left[1 - \cos \theta\right] \frac{N+1}{2} = z^N(1-z) \frac{N+1}{2}. \end{aligned} \quad (48)$$

This function behaves as an exponential function near $\theta = \pi$ ($z = -1$) (see Fig.18):

$$W_{-J}(z, \phi)|_{z \approx -1} \approx N \exp[-N(1+z)]. \quad (49)$$

Appendix B: Poincare surfaces of section for the Dicke model with counterrotating terms

Below we present Poincare surfaces of section of the Dicke model with counterrotating terms demonstrating: (i) chaoticization of large part of the phase space (ii) remaining regular parts near stable equilibria.

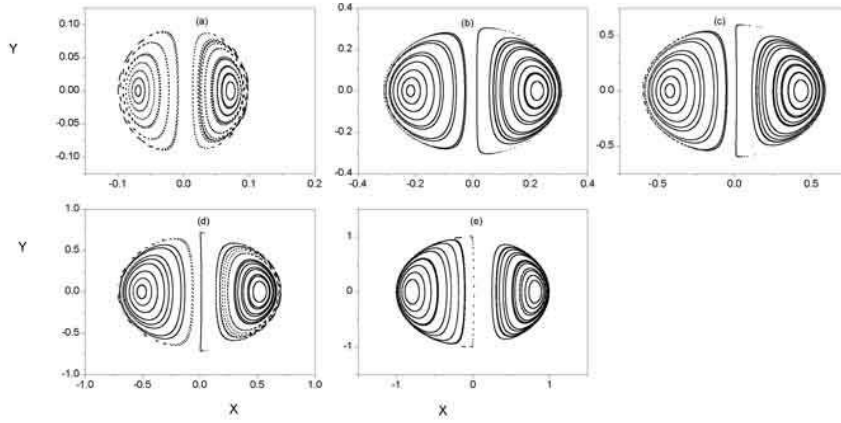


FIG. 19: Poincaré surfaces of section, weak coupling $\lambda = 0.02$. Different energy surfaces are shown: $h = -0.995, -0.95, -0.8, -0.7, 0.0$ for (a-e), correspondingly.

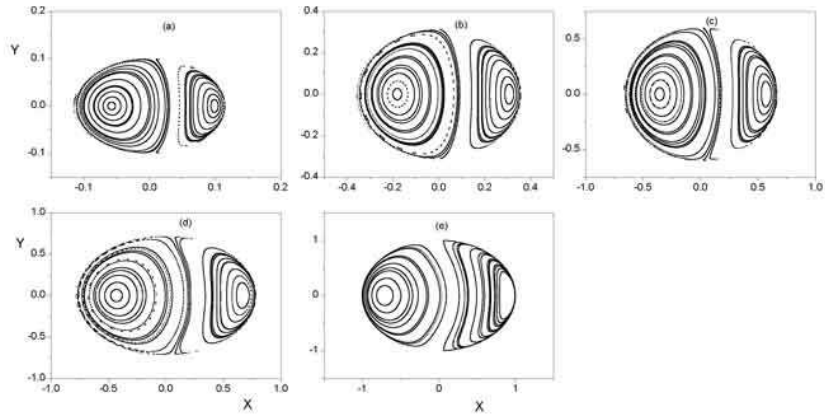


FIG. 20: Poincaré surfaces of section, $\lambda = 0.25$.

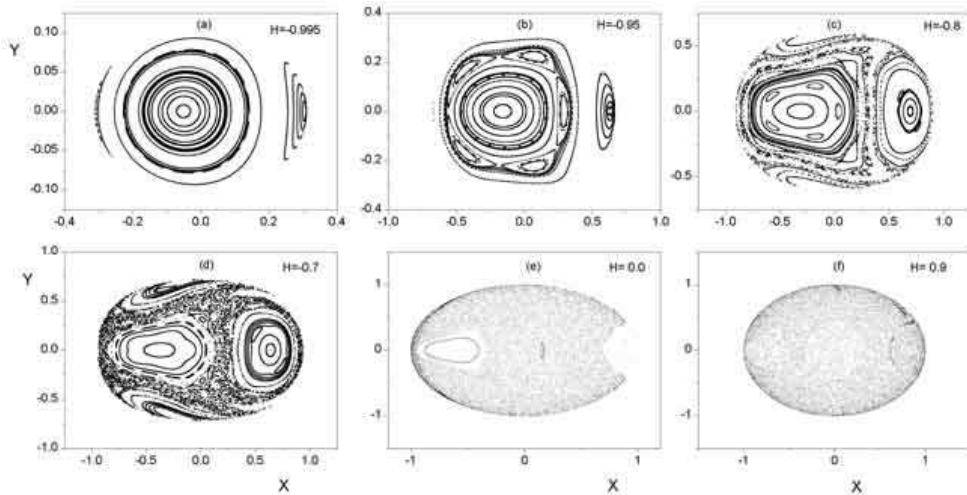


FIG. 21: Poincaré surfaces of section, $\lambda = 0.48$ (close to critical).

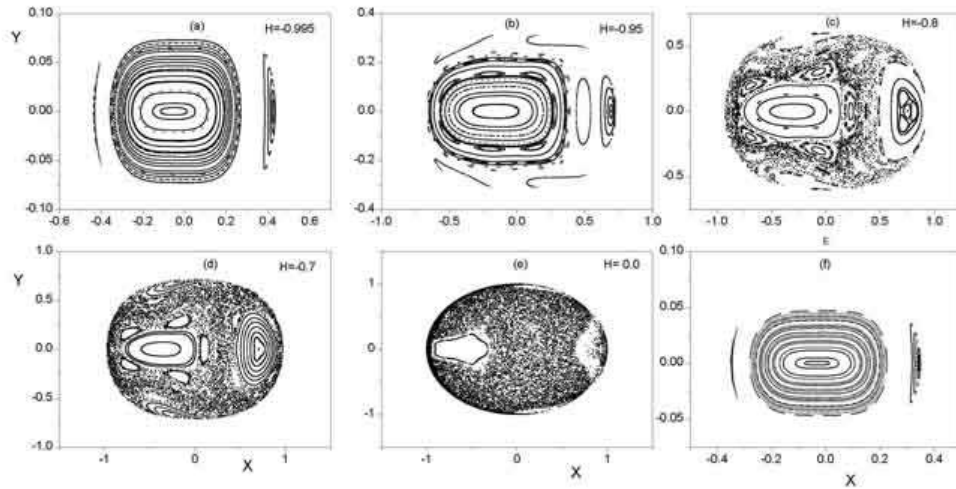


FIG. 22: Poincaré surfaces of section, $\lambda = 0.5$.

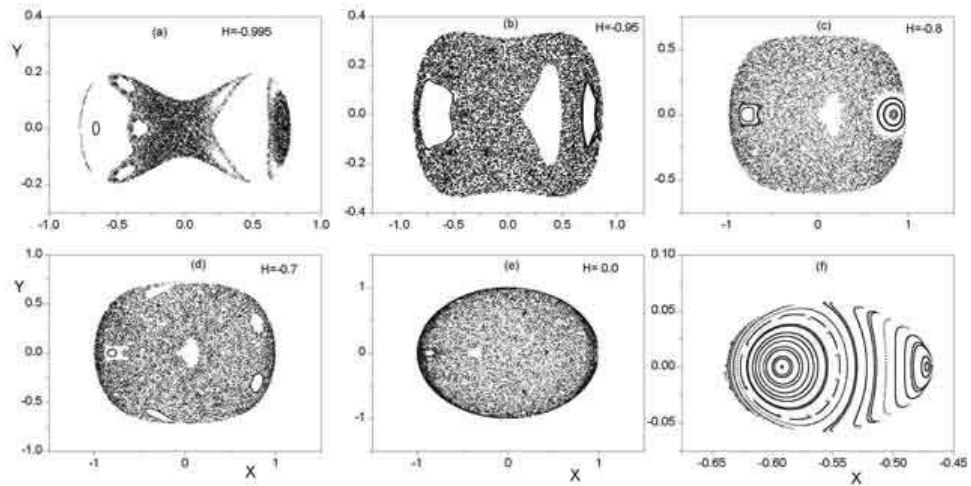


FIG. 23: Poincaré surfaces of section, $\lambda = 0.55$. Note that Fig. (f) corresponds to an energy level close to that of new equilibria. Poincaré surface of section is regular there.

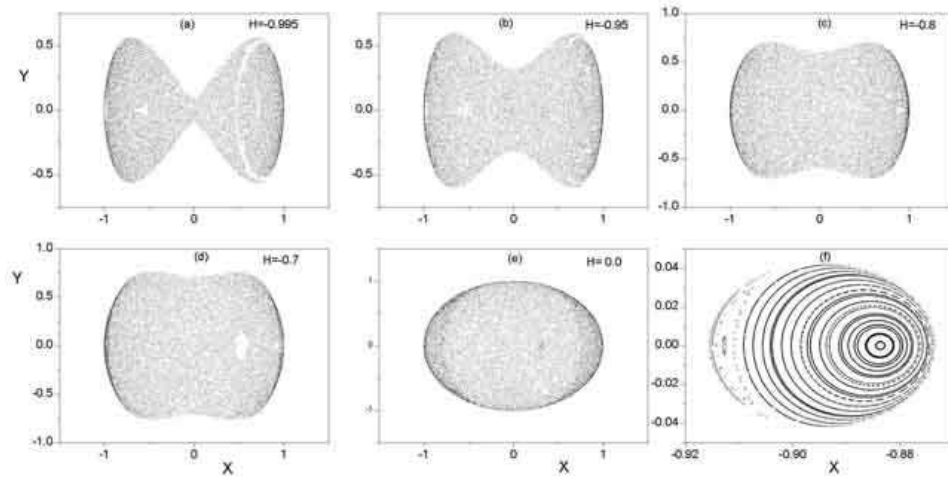


FIG. 24: Poincaré surfaces of section, $\lambda = 0.75$. Note that Fig. (f) corresponds to an energy level close to that of new equilibria. Poincaré surface of section is regular there.

Appendix C: mapping to Painleve equation in the Dicke model with counterrotating terms

Let us firstly do a canonical transformation to variables $(P_Y, Y), (P_X, X)$: $P_Y = \sqrt{2(1+z)}\sin\theta$, $Y = -\sqrt{2(1+z)}\cos\theta$, $P_X = p$, $X = e$. In the new variables

$$H = \frac{\omega}{2}(P_X^2 + X^2) + \frac{1}{2}(P_Y^2 + Y^2) - 2\lambda XY \sqrt{1 - \left(\frac{P_Y^2 + Y^2}{4}\right)}$$

Before the bifurcation, the equilibrium is in the origin. Near the origin, expanding the term with a square root in H in Taylor' series, we obtain approximately the equations of motion

$$\begin{aligned} \dot{P}_X &= -\omega X + 2\lambda Y \left(1 - \frac{P_Y^2 + Y^2}{8}\right) \\ \dot{X} &= \omega P_X \\ \dot{P}_Y &= -Y + 2\lambda X \left(1 - \frac{P_Y^2}{8} - \frac{3Y^2}{8}\right) \\ \dot{Y} &= P_Y + \lambda XY \frac{P_Y}{2}. \end{aligned} \quad (50)$$

Analyzing fixed points of the Hamiltonian, it is not difficult to see that at $\lambda = \lambda_{crit} = \frac{1}{2}$ a bifurcation happens and new equilibria at $Y = \sqrt{2\left[1 - \frac{\omega}{(2\lambda)^2}\right]}$, $P_Y = 0$, $P_X = 0$, $X = \pm \frac{2\lambda}{\omega} \sqrt{1 - \frac{\omega^2}{(2\lambda)^4}}$ emerge.

From now on, consider the case $\omega = 1$ for simplicity. Introducing the new variables $\tilde{P}_X = \sqrt{\omega}P_X$, $\tilde{X} = X/\sqrt{\omega}$, and making a rotation

$$\tilde{X} = (q_1 + q_2)/\sqrt{2}, \quad Y = (q_2 - q_1)/\sqrt{2}, \quad (51)$$

we obtain

$$\begin{aligned} H &= \\ &\frac{1}{2}(p_1^2 + p_2^2 + q_1^2 + q_2^2) + \lambda(q_1^2 - q_2^2) + \frac{\lambda}{16}(q_2^4 - q_1^4) + \\ &\frac{\lambda}{16}(q_2^2 - q_1^2)(p_1^2 + p_2^2 - 2(p_1 p_2 + q_1 q_2)). \end{aligned} \quad (52)$$

In a vicinity of the critical point $\lambda = \frac{1}{2}$, the effective Hamiltonian is

$$H = \frac{p_1^2}{2} + \frac{q_1^2}{2}(1 + 2\lambda) + \frac{p_2^2}{2} + \frac{q_2^2}{2}(1 - 2\lambda) + \frac{\lambda}{16}q_2^4. \quad (53)$$

Shifting the origin of time, approximating the change in λ by a linear law in the vicinity of the critical value $\lambda = \frac{1}{2} + \epsilon t$, and neglecting time dependence in the coefficient $1 + 2\lambda$, we obtain:

$$H = \frac{p_1^2}{2} + q_1^2 + \frac{p_2^2}{2} - \frac{q_2^2}{2}(2\epsilon t) + \frac{1}{32}q_2^4. \quad (54)$$

Neglecting the time dependence in the coefficient $1 + 2\lambda$ does not prevent one from obtaining correct lowest-order approximation of destruction of adiabaticity, since the change in the adiabatic invariants mostly happens around the time of bifurcation. Introducing new variables and rescaling the Hamiltonian as

$p_2 = 8P$, $p_1 = 8P_1$, $q_2 = 4\sqrt{2}Q$, $H = 64H'$, we obtain the Hamiltonian

$$H' = 32(P_1^2 + Q_1^2) + \frac{P^2}{2} + \frac{Q^4}{2} - \epsilon t \frac{Q^2}{2}. \quad (55)$$

Sweep through the bifurcation results in change of the adiabatic invariant analogous to that considered in Sections II-III.

Let us calculate quantitatively effects of non-adiabaticity averaged over the classical ensemble. We see in Fig.17 that after the sweep the photon number oscillates around a (time-averaged) mean value $n_0(\epsilon) = \langle \bar{n} \rangle$. Increasing the sweeping rate ϵ leads to shift of the mean value n_0 . The magnitude of this shift can be used to quantify the deviation from adiabaticity in the quasiclassical ensemble. Indeed, consider a single trajectory of the Hamiltonian $h = \frac{p^2}{2} - A\frac{q^2}{2} + B\frac{q^4}{4}$ (the effective final Hamiltonian after the sweep). It is easy to see that the magnitude of $\bar{n} = \frac{1}{4}(p^2 + q^2)$ in the first approximation linearly depends on the action of the trajectory I : $\bar{n} = \alpha - \beta I$. Explicit values of the coefficients α, β can be obtained from the following estimates:

(i) the relation between the action I and the energy h near a stable fixed point:

$$\begin{aligned} I &= \frac{1}{\pi} \int_{q_1}^{q_2} p dq = \frac{1}{\pi} \int_{x_1}^{x_2} \sqrt{2h + Ax - \frac{Bx^2}{2}} \frac{dx}{2\sqrt{x}} \\ &= \frac{1}{3\pi} \sqrt{\frac{Bx_2}{2}} [(x_2 + x_1)E(m) - 2x_1K(m)] \approx \frac{x^2}{4\sqrt{2AB^2}}, \end{aligned} \quad (56)$$

where

$$x_{1,2} = q_{1,2}^2 = \frac{A \mp x}{B}, \quad x = \sqrt{A^2 + 4Bh}, \quad (57)$$

and $m = \frac{x_2 - x_1}{x_2}$.

(ii) time-averaged magnitudes of p^2, q^2 :

$$\begin{aligned} \overline{q^2} &= \frac{1}{T} \int q \frac{dq}{\dot{q}} = \frac{1}{T} \int_{x_1}^{x_2} \frac{dx \sqrt{x}}{\sqrt{2h + Ax - \frac{B}{2}x^2}} \\ &= x_2 \frac{E(m)}{K(m)} \approx \frac{A}{B} - \frac{x^2}{4AB}, \end{aligned} \quad (58)$$

$$\overline{p^2} = \frac{1}{T} \int_{x_1}^{x_2} dx \frac{\sqrt{2h + Ax - \frac{B}{2}x^2}}{\sqrt{x}} \approx \frac{x^2}{4B}, \quad (59)$$

where the period $T = \int_{x_1}^{x_2} \frac{dx}{\sqrt{x} \sqrt{2h + Ax - \frac{B}{2}x^2}} = \frac{2}{\sqrt{x_2}} \sqrt{\frac{2}{B}} K(m)$.

We have therefore

$$\begin{aligned}\bar{n} &= \frac{1}{4}(p^2 + q^2) \approx \frac{1}{4B} \left(A + x^2 \left(\frac{1}{4} - \frac{1}{4A} \right) \right) \\ &= \frac{1}{4B} \left(A + IB\sqrt{2A} \left(1 - \frac{1}{A} \right) \right).\end{aligned}\quad (60)$$

One can note that \bar{n} is linearly proportional to the excess energy of a trajectory (i.e. the difference between the energy of the final solution and the adiabatic solution), which is often used for quantifying non-adiabaticity.

After averaging over the classical TWA ensemble,

$$\langle \bar{n} \rangle = \frac{A}{4B} + \langle I \rangle \sqrt{\frac{A}{8}} \left(1 - \frac{1}{A} \right), \quad (61)$$

where $\langle I \rangle$ is the mean value of the adiabatic invariant associated with the variables p_2, q_2 . We see that the (ϵ -dependent) shift of \bar{n} gives a convenient quantitative measure of the nonadiabaticity. If the sweep of λ ends at some magnitude λ_f being close to the critical one $\lambda_f = \frac{1}{2} + \delta\lambda_f$, $\delta\lambda_f \ll 1$, we have

$$\langle \bar{n} \rangle \approx \frac{A}{4B} - \langle I \rangle \frac{1}{\sqrt{8A}} = 4\delta\lambda_f - \frac{\langle I \rangle}{4\sqrt{\delta\lambda_f}}. \quad (62)$$

Let us find now the ϵ -dependence of $\langle I \rangle$.

The action I_2 of the Hamiltonian (53) is related to the action I_{PQ} of the Hamiltonian (55) as $I_2 = 32\sqrt{2}I_{PQ}$.

The final action I_2 of a trajectory from the classical TWA ensemble is related to its initial action as

$$I_2^+ \approx \frac{3}{4}I_2^- - \frac{8\sqrt{2}\epsilon}{\pi} \ln \left(\frac{2\pi I_2^-}{32\sqrt{2}\epsilon} \right). \quad (63)$$

Averaging over the TWA ensemble leads to

$$\langle I_2 \rangle = \frac{3}{4N} + \frac{8\sqrt{2}\epsilon}{\pi} \left(C_\gamma + \ln \left(\frac{2N\epsilon 8\sqrt{2}}{\pi} \right) \right). \quad (64)$$

Substituting this expression into Eq.62 in place of $\langle I \rangle$, we obtain the theoretical prediction for the shift of the mean photon number n . Note that we do not consider $1/N$ differences between quantum observables and semiclassical TWA ones, but only present the TWA-Painleve prediction for the semiclassical ensemble. This prediction is compared with TWA numerics for $N = 500$ and $\delta\lambda_f = 0.03$ in Fig.17. Remarkable coincidence can be seen at slow sweeps.

-
- [1] V.I. Arnold, V.V. Kozlov, and A.I. Neishtadt, *Mathematical aspects of classical and celestial mechanics* (Third Edition, Springer, Berlin, 2006).
- [2] P.Ehrenfest, *Verh. Dtsch. Phys. Ges.* **15**, 451 (1913); P.Ehrenfest, *Ann.Phys.* **51**, 327 (1916); P. Ehrenfest, *Phil. Magazine* **33**, 500 (1917)
- [3] L. Navarro and E. Perez, *Arch. Hist. Exact Sci.* **60**, 209 (2006).
- [4] P.A.M. Dirac, *Proc. Roy.Soc.* **107**, 725 (1925).
- [5] M. Born, *Z.Phys.* **40**, 167 (1926); M. Born, V. Fock, *Z. Phys.* **51**, 165 (1928).
- [6] E. Fermi, E. Persico, *Rend. Accad. Lincei*, 4, 452 (1926); E. Fermi, *Note e Memorie (Collected Papers)*, Edited by E. Amaldi et al. (Accademia nazionale dei Lincei-University of Chicago Press, Roma-Chicago 1962-65).
- [7] I. Bloch, J. Dalibard, and W. Zwerger, *Rev. Mod. Phys.* **80**, 885 (2008); S. Giorgini, L.P. Pitaevskii, and S. Stringari, *ibid* **80**, 1215 (2008).
- [8] E.A. Donley et al, *Nature* 417, 529 (2002); C.A.Regal, M.Greiner, and D.S. Jin, *Phys.Rev.Lett* **92**, 040403 (2004); M.W.Zwierlein et al, *ibid*, 92, 120403 (2004); E. Hogby et al, *ibid* **94**, 120402 (2005);
- [9] L. Landau, *Phys. Z. Sowj.* **2**, 46 (1932); C. Zener, *Proc. R. Soc.* **137**, 696 (1932).
- [10] G.J.Milburn et al, *Phys. Rev. A* **55**, 4318 (1997); J.I.Cirac et al, *ibid.* **57**, 1208 (1998); G.S. Paraoanu, S.Kohler, F.Sols, A.J.Legett, *J.Phys. B* **34**, 4689 (2001); O.Zobay and B.M. Garraway, *Phys. Rev. A* **61**, 033603 (2000); A.Micheli et al, *ibid.* **67**, 013607 (2003); O. Morsch et al, *ibid.* **67**, 031603 (2003); F.K. Abdullaev et al, *ibid.* **67**, 013605 (2003); A.K. Tuchman et al, *ibid.* **74**, 051601 (2006); H.Saito et al, *ibid.* **76**, 043613 (2007); H.Saito et al, *ibid.* **76**, 053619 (2007); T.-L. Horng et al, *ibid.* **79**, 053619 (2009).
- [11] J. H. Huckans et al, arXiv:0901.1386; M. V. Berry and D. H. J. O'Dell, *J. Phys. A* 32, 3571 (1999).
- [12] A. Altland *et al.*, *Phys.Rev. A* **79**, 042703 (2009).
- [13] A.P. Itin *et al.*, *Physica D* **232**, 108 (2007).
- [14] A.P. Itin, P. Törmä, *Phys. Rev. A* **79**, 055602 (2009).
- [15] E.Wigner, *Phys. Rev.* **40**, 749 (1932).
- [16] J.P. Dowling, G.S. Agarwal, W.P. Scheich, *Phys. Rev. A* **49**, 4101 (1994); G.S. Agarwal, R.R. Puri and R.P. Singh, *Phys. Rev. A* **56**, 2249 (1997).
- [17] A.B. Klimov, S.M. Chumakov, *Rev. Mex. Fis* **48**, 317 (2002).
- [18] P. Painlevé, *Acta Mathematica* **25**, 1 (1902).
- [19] A.S. Fokas, A.R. Its, A.A. Kapaev and V.Yu. Novokshenov, *Painleve' Transcendents: A Riemann-Hilbert Approach*, AMS (2006).
- [20] S.Kowalevski, *Acta Mathematica* **12**, 177 (1889); *ibid*, **14**, 81 (1890).
- [21] D.L. Vainshtein, L. M. Zelenyi, A. I. Neishtadt, and B. V. Savenkov, *Plasma Phys. Rep.* **25**, 299 (1999).
- [22] R.H. Dicke, *Phys. Rev.* **93**, 99 (1954).
- [23] H.J. Lipkin, N. Meshkov, and A.J. Glick, *Nucl. Phys.* **62**, 188 (1965).
- [24] J. Keeling and V.Gurarie, *Phys. Rev. Lett* **101**, 033001 (2008); A. Altland, V. Gurarie, *ibid* **100**, 063602 (2008).
- [25] K. Baumann, C. Guerlin, F. Brennecke, T. Esslinger; *Nature* **464**, 1301 (2010).
- [26] J. Larson, *EPL* **90**, 54001 (2010).
- [27] E.Emary, T. Brandes, *Phys. Rev. Lett* **90**, 044101 (2003);

- E. Emary, T. Brandes, Phys. Rev. **E 67**, 066203 (2003).
- [28] E. Timmermans, P. Tommasini, M. Hussein, and A. Kerman, Phys. Rep. **315**, 199 (1999).
- [29] J. Javanainen and M. Mackie, Phys. Rev. **A 59**, R3186 (1999); M. Kostrun et al, *ibid* **62**, 063616 (2000).
- [30] T. Köhler, K. Góral, P.S. Julienne, Rev. Mod. Phys. **78**, 1311 (2006).
- [31] E. Altman and V. Vishwanath, Phys. Rev. Lett. **95**, 110404 (2005); R. Barankov, L. Levitov, e-print arXiv:cond-mat/0506323.
- [32] V. Gurarie, Phys. Rev. **A 80**, 023626 (2009).
- [33] E.M. Chudnovsky, and D.A. Garanin, Phys. Rev. Lett **89**, 157201 (2002); O. Shafir, A. Keren, Phys. Rev. **B 79** 180404 (2009); J. Tejada et al, Appl. Phys. Lett **84** 2373 (2004).
- [34] A.V. Shytov, Phys. Rev. **A 70**, 052708 (2004).
- [35] C.W. Gardiner et al, J. Phys. **B 35**, 1555 (2002).
- [36] A. Polkovnikov, Phys. Rev. **A 68**, 033609 (2003).
- [37] $\tilde{n} = w = 1 - 2n$, $\tilde{\phi} = \pi - \phi$, $\tilde{H} = \sqrt{2}H$, $\tilde{t} = \sqrt{2}t$, $\tilde{\delta} = \gamma/\sqrt{2}$.
Omitting tildes, now $H = \delta(w - 1) + (1 - w)\sqrt{1 + w \cos \phi}$
- [38] J.R. Cary, D.F. Escande, and J. Tennyson, Phys. Rev. **A 34**, 4256 (1986).
- [39] A.I. Neishtadt, Sov. J. Plasma Phys. **12**, 568 (1986).
- [40] A.R. Its and A.A. Kapaev, Izv. Akad. Nauk SSSR, Ser. Mat. **51**, 878 (1987).
- [41] H. Flashka, A.C. Newell, Comm. Math. Phys. **76**, 65 (1980); A.S. Fokas and M.J. Ablowitz, *ibid.* **91**, 381 (1983); V. Yu. Novokshenov, Funkts. Anal. Prilozhen. **18**, 90 (1984).
- [42] Formally, classical system is deterministic: initial conditions and equations of motion are fixed. Nevertheless, fate of an individual classical trajectory is highly dependent on the initial phase (being uniformly distributed), and therefore is "quasi" random. Probabilistic phenomena in dynamical systems were discussed, e.g., in [1, 43].
- [43] V.I. Arnold, Russ. Math. Surv. **18**, 85 (1963); A.I. Neishtadt, Celest. Mech. Dyn. Astron. **65**, 1 (1997).
- [44] A. Ishkhanyan *et al.*, Phys. Rev. **A 69**, 043612 (2004).
- [45] U. Fano, Phys. Rev. **124**, 1866 (1961); Y. S. Joe, A. M. Satanin, and C. S. Kim, Phys. Scr. **74**, 259 (2006); A.E. Miroshnichenko, S. Flach, and Y.S. Kivshar arXiv:0902.3014.
- [46] A. Polkovnikov, Phys. Rev. **B 72**, 161201(R) (2005); E. Altman et al, Phys. Rev. Lett. **95**, 020402 (2005); A. Polkovnikov and V. Gritsev, Nat. Phys. **4**, 477 (2008).
- [47] W.H. Zurek, U. Dorner, and P. Zoller, Phys. Rev. Lett. **95**, 105701 (2005); J. Dziarmaga, *ibid* **95**, 245701 (2005); R. Schützhold et al., *ibid* **97**, 200601 (2006).
- [48] J. Dziarmaga, arXiv:0912.4034 (Adv. in Physics).
- [49] S. Mondal et al, Phys. Rev. **B 78**, 045101 (2008); T. Caneva et al, Phys. Rev. **B 76**, 144427 (2007).
- [50] J. Keeling, M. J. Bhaseen, and B. D. Simons, arxiv:1002.3108
- [51] T. Caneva, R. Fazio, G. Santoro, Phys. Rev. **B 78**, 104426 (2008).
- [52] P. Solinas, P. Rubeiro, R. Mosseri, Phys. Rev. **A 78**, 052329 (2008).
- [53] J. Vidal, G. Palacios, C. Aslangul, Phys. Rev. **A 70**, 062304 (2004).
- [54] A.M. Dykhne, Sov. Phys. JETP **11**, 411 (1960).
- [55] M. Kitagawa, M. Ueda, Phys. Rev. **A 47**, 5138 (1993).
- [56] K. Furuya et al, Phys. Rev. Lett **80**, 5524 (1998).
- [57] I.L. Kirilyuk and S.V. Prants, Optics and Spectroscopy **89**, 901 (2000).